# *Ab Initio* Investigations of Gas Adsorption on Buckybowls

by

**Daniel J. Burrill**

Bachelor of Science, Michigan Technological University, 2012

Master of Science, University of Vermont, 2015

Submitted to the Graduate Faculty of

the Dietrich School of Arts and Sciences in partial fulfillment

of the requirements for the degree of

**Doctor of Philosophy**

University of Pittsburgh

2020

UNIVERSITY OF PITTSBURGH

DIETRICH SCHOOL OF ARTS AND SCIENCES

This dissertation was presented

by

Daniel J. Burrill

It was defended on

March 27, 2020

and approved by

Dr. Daniel Lambrecht, Department of Chemistry

Dr. Kenneth Jordan, Department of Chemistry

Dr. Susan Fullerton, Department of Petroleum and Chemical Engineering

Dr. Alexander Star, Department of Chemistry

Dissertation Director: Dr. Daniel Lambrecht, Department of Chemistry

***Ab Initio* Investigations of Gas Adsorption on Buckybowls**

Daniel J. Burrill, PhD

University of Pittsburgh, 2020

Gas separation processes are prevalent in science and industries to isolate desired or remove undesired gases from mixtures. Of the various methods to perform this separation, surface adsorption has been shown to be a promising avenue due to favorable temperature and pressure limits, high capacity, and chemical tunability. This thesis focuses on using a carbon-based, bowl-like molecule known as a Buckybowl to act as a gas adsorbent. The bowl-like nature of this structure has been shown to have stronger dispersion and electrostatic interactions on the concave side suggesting that it is a potential candidate for gas capture and release systems. In this study, the small gas molecules $CH_4$, $CO_2$, NO, and $NO_2$ are explored computationally as adsorbates on to the Buckybowls corannulene and sumanene as well as the planar structure coronene. It is found that the bowl-up orientation of the Buckybowls, with respect to the adsorbate, has the strongest interaction energy (sumanene $CH_4$, -5.6 kcal/mol) followed by coronene (-2.9 kcal/mol) and then the bowl-down configurations (sumanene $CH_4$, -1.8 kcal/mol). Sumanene was found to have the strongest adsorption energies for these molecules (BU $CO_2$, -6.1 kcal/mol) with binding to corannulene (BU $CO_2$, -4.8 kcal/mol) and coronene ($CO_2$, -3.7 kcal/mol) being weaker. The system studied were also found to exhibit stimulus-induced adsorption/desorption. Specifically, the Buckybowls were found to change selectivity towards specific adsorbates in response to an applied electric field as the interaction energy ordering was altered. Beyond atmospheric molecules, the ability of sumanene to adsorb respiratory irritants was also explored. It was found that for three potent irritants, 2-chlorobenzalmalonitrile, 1,6 hexamethylene diisocyanate, and toluene diisocyanate, the interaction energies are about -14 kcal/mol with attraction largely driven by electrostatic and dispersion effects. No significant energetic barriers due to structural changes were found indicating that sumanene could be a possible gas capture system for these chemical compounds.

## Table of Contents

## List of Tables

## List of Figures

# Preface

**Further, science is a collaborative effort. The combined results of several people working together is often much more effective than could be that of an individual scientist working alone.**

***John Bardeen***
*Stockholm, 1972*

The goal of this thesis is to investigate Buckybowls as possible adsorbent materials for a range of gaseous molecules. To achieve this, a computational study was undertaken to identify interaction strengths, the components contributing to the interaction energy, and determine whether an external electric field could be used to influence selectivity of the adsorption process. As is typically found in the gas separation literature, the motivation was to identify sensitive, selective, and stable devices which could be chemically altered to fit the situation at hand.

Chapter 1 presents an introduction to the topic of gas separation as found within industry and presents several methods currently employed. Special care is given to identifying the advantages and disadvantages to each method to highlight the usefulness of using surface adsorption systems which can be chemically tuned, have high capacities, and have operating conditions in a desirable range. Chapter 2 then describes the main features of the theory used to perform the calculations in the following chapters. A general introduction to density functional theory is given with emphasis on the practical side of performing the calculations and indications of the input to such computations. This is followed by a derivation of the terms of polarization theory which was the precursor to standard symmetry adapted perturbation theory (SAPT). Here I tried to be as transparent as possible at each step to help the reader understand exactly how perturbation theory is used to decompose the components of an interaction into useful terms such as electrostatics, induction, and dispersion. Then a short introduction to absolutely localized molecular orbitals (ALMO) is given where the aim was to introduce the definitions of different binding contributions and contrast the relative simplicity of the method with SAPT. It is important to note that there are numerous different methods based on localized orbitals so I have chosen to only describe the method used in calculations within this thesis.

Following the theory, Chapters 3 and 4 are computational investigations into the interaction properties of small gas molecules and three highly potent respiratory irritants. The small gas molecules were chosen for their importance as green house gases and atmospheric pollutants. Controlling their concentrations help alleviate environmental issues while the respiratory irritants are important for developing technologies for reducing workplace exposure to hazardous chemicals. Interaction energies are explored through the use of energy decomposition analysis to determine the components of the interaction which contribute the most to the attractive or repulsive nature of the adsorption process. Finally, a conclusion is provided to give a quick overview of the result and inform the reader about possible future directions of this work.

Throughout the thesis process there are numerous people I am indebted to for providing their time, expertise, and insights. First, I would like acknowledge the patience of my advisor and co-advisor Drs. Daniel Lambrecht and Ken Jordan who have spent numerous hours discussing computational details and helping to forge projects into well thought-out ideas. I would like to thank Dr. Ping Yang for being instrumental all throughout my graduate career for providing advice and insight into graduate studies and opportunities outside of academia. Due to their patience and great managerial expertise I would also like to thank Drs. Jeff Gearhart and Heather Pangburn for providing me the opportunity to explore data science and machine learning with an extraordinary group of researchers and friends. Thank you to the members of the Lambrecht group, Drs. Keith Werling and Eric Berquist, for the countless conversations about science and dinosaurs as well as to the members of the Jordan group for being willing to discuss the minute details of the computational sciences. Finally, I would like to thank the most important person of all - my wife, Dr. Kim Burrill, who has been enormously patient over these past few months during the writing process when I am absent minded or thinking about research.

## 1.0 Introduction

> **It has been shown that in the case of two hydrogen atoms in the normal state brought near each other the eigenfunction which is symmetric in the positional coordinates of the two electrons corresponds to a potential which causes the two atoms to combine to form a molecule.**
>
> ***Linus Pauling***
> *The Shared Electron Chemical Bond, 1928*

The overall objective of this thesis is to provide insights into the adsorption characteristics of gas molecules with Buckybowls. These molecules can be imagined as sections removed from the larger Buckyball as shown in Figure 1 capped with hydrogen atoms. Before describing how Buckybowls possess properties amenable to the gas separation process, a brief introduction to the fascinating origin of Buckyballs will be presented followed by a short survey of the gas separation field.

Below the tail of the constellation Scorpius lies a large collection of gases driven outward by stellar winds. This planetary nebula, labeled Tc 1, formed as a red giant passed through the asymptotic giant branch phase of its life. Initially, the rate of hydrogen fusion in the core of the star slowly decreased until it could no longer sustain a balancing force against gravity. Under great pressure, higher temperatures from the core transferred energy into the lighter gases surrounding the star causing it to expand into a red giant. Helium fusion then proceeded when the core reached a critical temperature resulting in the creation of carbon and oxygen. These heavier elements coalesced into a stable core surrounded by burning helium and a thin shell of the lighter hydrogen. As the supply of helium depleted, the thermal energy from the core began to transfer to the hydrogen gases, reigniting the fusion process. This interplay between hydrogen and helium fusion reactions continued with interesting side effects. As the burning hydrogen produced more helium, the helium in turn began to fuse causing a violent reaction near the surface of the core. Carbon and oxygen atoms were driven up through the gases and pushed outwards creating the planetary nebula we see today.

The gases disperse throughout the interstellar medium and are typically composed of

polyaromatic hydrocarbons (PAHs) and compounds containing heavier elements such as SiC. In 2010, NASA's Spitzer Space Telescope recorded an infrared spectrum from Tc 1 that was contrary to expectation - rather than containing spectra indicative of PAHs, strong signals were present at 7.0, 8.5, 17.4, and 18.9 $\mu$m. Infrared signals from these gases have been studied for decades as researchers try to understand their composition. In particular, Kroto *et al.* were the first to propose that the $C_{60}$ fullerene (colloquially known as a Buckyball) molecule could account for these peaks, but the conditions under which they were formed in stars was not completely understood [1]. Cami *et al.* provided a key insight by analyzing the data from Tc 1 and found that these signals coincided with the spectral peaks observed for $C_{60}$ when present in a helium gas [2]. Through the process of creating planetary nebulae, Buckyballs are forged from the shattered remains of carbon-rich cores and ejected into the universe to be scattered by stellar winds. Tc 1 provided a unique environment for the creation of $C_{60}$, and to a lesser extent $C_{70}$, fullerenes since it had apparently shed most of its outer hydrogen shell long before the carbon was exposed by helium shell flashes. This corresponds with the hydrogen-depleted, carbon-rich environment required in the laboratory for creating fullerenes through vaporizing graphite.

In 1996, the Nobel prize in Chemistry was awarded to Robert Curl, Sir Harold Croto, and Richard Smalley for their discovery of the Buckminster fullerene motivated by understanding the composition of interstellar gas clouds [1]. Since then, the molecule has been studied extensively and has seen use in many chemical applications. The 20 hexagons and 12 pentagons that comprise the Buckyball offer a wide variety of rich chemistries while the cage-like structure opens the possibility to many types of endofullerenes.

This work is focused on sections of the Buckyball molecule known as Buckybowls. These molecules are derived from parts of $C_{60}$ fullerene centered at either the pentagon or hexagon. The aromatic nature of the carbon bonds coupled with the bowl-like shape of the molecules offer interesting physical properties that make them targets for research into their adsorption characteristics. In particular, the ability of these Buckybowls to act as gas capture/release systems shows promise by being sensitive to gas adsorption on the concave side, selective in gas mixtures under an external electric field, and recyclable through inversion of the bowl in the sense that interaction energies are significantly weaker on the convex side for small gas

molecules.

## 1.1 Gas Separation

Before expounding the details of how Buckybowls are potential gas separation candidates, it would be useful to step back and look at the current state of the field. Gas separation processes are used for isolating or removing components of a gas mixture as well as analysis and detection of specific compounds. The separation of atmospheric pollutants and green house gases from industrial emissions represents one application. In the Unites States alone, about 5,300 million metric tons of $CO_2$ are generated as the result of various industrial processes. Electricity generation accounts for about a third of this with coal-fired power plants contributing the majority of $CO_2$ [3]. Significant potential exists for creating and utilizing technologies for capturing the $CO_2$ to reduce emissions and use for commercial purposes. Southwest of Houston a coal-fired facility, the WA Parish power plant, was fitted for exactly this purpose. In 2016, work on a carbon capture system (CCS) was completed on their number 8 unit which was partially financed by the U.S. Department of Energy as a pilot project to test the efficacy of CCSs at major industrial sites. Normally this unit would emit about 1.1 million tons of $CO_2$ per month into the atmosphere, but after the CCS was deployed this was reduced by 90% [4]. The Kansai Mitsubishi carbon dioxide recovery (KMCDR) process was employed which relies on the use of amine-based solvents to absorb the $CO_2$ and then recycle for later use [5]. The $CO_2$ is then piped from the power plant to an oil field 80 miles away where the gas is used to improve the production efficiency of oil extraction. This is just one example that shows how gas capture and release systems are a proven method of reducing emissions from large industrial facilities as well as generating positive economic results.

Numerous methods are in use as gas capture/release systems. Some, such as chemical absorption, have been in use for over a hundred years. Below is a brief description of the important gas capture/release methods in use today.

### 1.1.1 Chemical Absorption

The KMCDR process as described above is a form of gas capture through chemical absorption. Gas is passed through an amine-based solvent which reacts with the $CO_2$ to yield a purified feed gas and a byproduct gas from which the $CO_2$ can be extracted for later use. Similarly, chemical absorption is widely used within the petroleum industry to extract sulfur compounds from petroleum residues. Products from crude oil are mainly extracted via distillation techniques. When oil is pumped from the ground, it is fed into a distillation tower where products separate based on their densities. Near the top of the tower, products such as kerosene and light oil are removed for further refinement while heavier products settle to the bottom. Since crude oil rarely consists of pure hydrocarbons, several contaminants can cause oil to settle at the bottom of the towers after all of the products have been removed - this is known as petroleum residue. Further processing is required to remove the contaminants and produce useful hydrocarbons.

One technique to refine the pertroleum residue is known as hydroconversion. This process takes the residue as an input feed and combines it with hydrogen gas to create useful hydrocarbons. During this process, sulfur-containing contaminants are extracted via chemical absorption with an amine solution. As mentioned, the feed components are passed through a heater and filter to promote chemical reactions in the catalytic reactors. Here the hydrocarbons are formed through a series of processes and then passed into a thermal separation unit. Within the thermal separation unit the useful components are passed into a distillation tower (fractionator) while gases containing the contaminants are passed into the absorption tank. Purified amine solution is fed in through the top of the tank while the gases rise through the solvent. Chemical reactions with the gas transfer the suflur compounds into the solvent creating so-called rich amines which can then be removed and recycled. Purified $H_2$ is then recycled from the absorption process and fed back into the start of the loop. Further processing is necessary to remove the sulfur compounds from the rich amine which is usually done through heating. Therefore, while the chemistry of chemical absorption is well known, significant amounts of energy are necessary to recycle the solvents and remove contaminants for other uses. Sensitivity and selectivity can be tuned through the choice of

chemical solvent, but in practice several passes through a processing step are required to remove all of the components desired.

### 1.1.2 Cryogenic Distillation

The basic principles behind cryogenic distillation are rooted in utilizing gas to liquid transitions to separate out the various components of a gas. Industrial facilities which use this method of gas separation typically produce liquid nitrogen, oxygen, and argon. The process begins compressing air from the atmosphere and removing the $H_2O$ and $CO_2$. The dry air is then passed into a cryogenic distillation tank where the gas is cooled by using the Joule-Thomson effect. The temperature of a compressed gas can be quickly reduced by passing it through a small valve and allowing it to rapidly expand. The temperature of the tank can be controlled to separate out specific components of the gas. For instance, the most accessible gas using this method is nitrogen. By cooling past 77 Kelvin the nitrogen becomes a liquid and the remaining gas yields low grade oxygen due to argon impurities. Reducing the temperature further allows creating of liquid oxygen and argon, but this process uses a considerable amount of energy for refrigeration. Overall, this method is highly effective at separating gases with considerably different gas-liquid transition temperatures; however, for gas mixtures with similar transition temperatures, such as argon and oxygen, this process is not efficient due to the need to use several cryogenic steps.

### 1.1.3 Membrane Filtration

The process of gas separation with membrane filtration relies on physically blocking unwanted components using permeable membranes. While best known for desalination of salt water, membrane filtration is also applied to separating gases. For instance, reserves of natural gas are often contaminated with high levels of $CO_2$ and $H_2S$ which need to be removed before distribution within the United States. Membrane filters are employed to capture the contaminant gas and leave behind an assortment of desired alkanes. Selectivity of these filters is controlled by the type of material chosen as the membrane. Polymers such as polysulfone and polyimides are employed in $H_2$ recovery while polycabonates and

polythenylene oxide are used in $N_2$ production to name a few [6]. However, the permeability and selectivity of the filter are often competing variables. While large pore sizes are critical to creating high throughput filters, the selectivity suffers because more gas molecules are allowed to pass through. This is commonly known as the Robeson trade-off and has a theoretical upper limit as defined by Robeson in 2008 [7]. It is important to note that while the Robeson is an important metric, efficiencies are not typically as good as predicted due to membrane degradation. Novel membrane structures are being actively developed in an effort to produce highly permeable and selective membranes for specific types of gas separation. Recent work using covalent organic frameworks (COFs) has been shown to be a promising avenue of exploration due to the ability to precisely control pore size and flexibility of design [8].

### 1.1.4 Surface Adsorption

Numerous candidates exist for adsorbing gas molecules to surfaces. Historically, metal oxides have played this role through chemisorption. Due to undesirable interactions with $H_2O$ molecules, gas separation from the surface of metal oxides is typically performed at temperatures exceeding 300° C and have been shown to be robust at higher temperatures [9]. Selectivity is governed by the type of oxide surface with metal coordination, acid-base reactions, and redox chemistry dictating the strength of interaction [10].

Other technologies have also been recently developed that focus on adsorption in specific gaseous environments such as zeolites and metal organic frameworks (MOFs). These materials focus on the porosity of their structures to increase the surface area to maximize adsorption effectiveness. In contrast to membrane filtration, surface chemistry is exploited by tailoring the structure and active groups present in the pores to suit a specific need. However, higher pressures are typically still required to force gas molecules though the pores. Zeolites are porous aluminosilicates with counter ions present. One popular form, known as X13, uses sodium as the counter ion and has shown desirable gas separation characteristics [11, 12]. While metal oxide surfaces require high temperatures to facilitate adsorption and recycling, zeolites can operate at room temperature with a recycling threshold between

150 and 180° C [13].

MOFs operate similarly to zeolites with a few distinguishing features. In a MOF, metal ions are connected through the use of organic ligands to form periodic structures. Due to the freedom to choose the organic ligands, structures of MOFs are significantly more customizable which allows tuning of both the sensitivity and selectivity. This is in contrast to zeolites which have a limited number of active groups which can bind to the surfaces of the pores. Additionally, the sizes of cavities in MOFs can be adjusted to increase the surface to volume ratio which ultimately provides a more efficient gas adsorber. At pressures above 10 bar, MOFs were found to have significantly higher active surface areas (1500-4500 $m^2g^{-1}$) compared to both activated carbon (400-1000 $m^2g^{-1}$) and zeolites (1500 $m^2g^{-1}$) [9]. Despite promising gas adsorption data, MOFs are generally more fragile than zeolite structures. Thermal instability and chemical degradation lead to MOFs being less utilized in industry.

## 1.2 Buckybowls for Adsorption

Since the discovery of $C_{60}$ fullerene in 1985 [1], significant research has been devoted to understanding the various allotropes of carbon in an effort to harness the interesting physics and high stability of carbon-based systems. In the 1990's, Buckyball thin films were of interest for adsorption of gases at low temperature. While the binding energy of an adsorbate to a single Buckyball is low, thin films of these molecules can be used to condense gases at low temperature in the gaps between them [14, 15, 16, 17, 18, 19, 20, 21].

The convex curvature of the Buckyball from the point-of-view of an adsorbate lends to its weak adsorption energy. Consider the case of a single gas molecule interacting with a graphene sheet where the interaction from local $\pi$-interactions and delocalized dispersion can be considered the baseline. If curvature is added to the graphene sheet, these interactions will change. In particular, as the sheet bends away from the molecule, $\pi$-interactions and dispersion with neighboring rings are reduced similar to the case of fullerenes. However, if the sheet bends towards the gas molecule, the trend of electronic interactions reverses. It is important to point out that increasing or decreasing $\pi$-interactions does not linearly

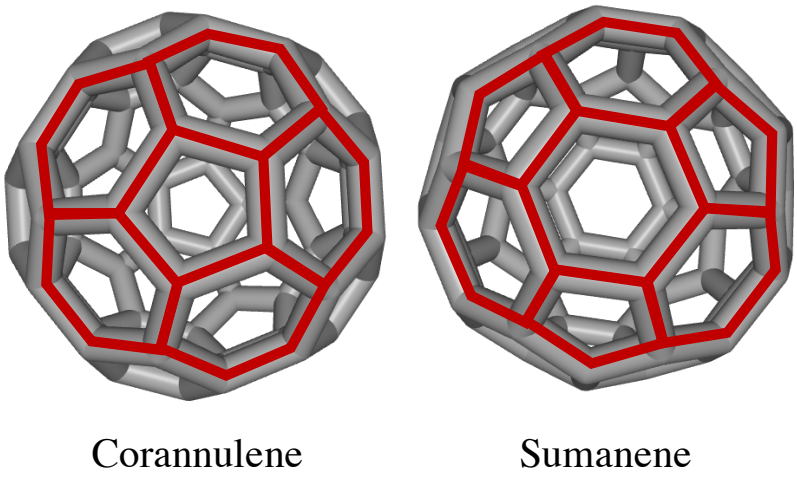


Figure 1: Structure of the corannulene and sumanene molecules superimposed in red on a Buckyball.

affect the total interaction energy. While attractive dispersion forces follow from increased $\pi$-interactions, so too does a repulsive force due to Pauli exclusion resulting in more complicated trends for total interaction energies. Each adsorbate-adsorbent case must be investigated on a case-by-case basis to discern the nature of the interaction.

Both cases of the curvature can be accessed by creating a Buckybowl. Figure 1 shows the outlines of the two smallest Buckybowls, corannulene and sumanene, on the profile of a Buckyball. Corannulene is the smallest Buckybowl and is distinguished by a central cyclohexane ring surrounded by five benzene rings. Sumanene is slightly larger and is composed of a central benzene ring with an outer ring of alternating benzene and cyclohexane rings.

Corannulene (Dibenzo[ghi,mno]fluoranthene) was first synthesized in 1966 by Barth and Lawton in a complicated liquid phase process with an effective yield of only about 1% [22]. Largely due to the complexity of the process, research proceeded slowly until new synthesis processes were discovered. Recently, large batch synthetic processes have been developed producing 1 kg of corannulene at a far more efficient 88% yield [23]. Similarly, synthetic processes for sumanene are also being developed to enable greater yields and more chemical flexibility such as adding functional groups [24, 25, 26, 27].

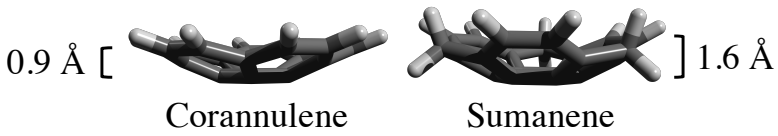


Figure 2: Profile images of the corannulene and sumanene bowls. The bowl depths are marked on the sides with corannulene at about 0.9 Å while sumanene has a depth of 1.6 Å and are measured as the vertical distance between the carbon atoms in the central ring to the carbon atoms in the outer ring. Note that the carbon atoms located at the rim of the bowl in sumanene do not have a uniform height from the bottom of the bowl. Therefore, the height is measured as the distance between the bottom and the highest carbon atom.

One of the most iconic features of a Buckybowl is the the bowl-like shape of the molecule. Figure 2 shows the profile of corannulene and sumanene with the labeled bowl depths. The bowl-like nature of these molecules lends two possible configurations for gas adsorption - bowl up (BU) where the concave side of the molecule is facing the adsorbate and bowl down (BD) which has the convex side towards the adsorbate. The transition between these two states is known as the inversion barrier and has been studied in the gas phase [28, 29, 30] as well as on surfaces [31, 32]. The gas phase inversion energy of corannulene was found to be about 10.2 kcal/mol [28] while sumanene was found to have a barrier of about 20.2 kcal/mol in solution [30].

Small molecules fit into the concave cavity leading to a large contact are for binding. Hussain *et al.* studied the interactions between small gas molecules and corannulene, sumanene, as well as coronene [33]. Coronene is a planar molecule of similar radius to corannulene, consisting of a central benzene ring surrounded by six other benzene rings. In particular, they investigated the interactions with $CO_2$, $CH_4$, and $C_2H_2$ which are industrial byproducts. From their computational results, they report two major findings. First, the binding energy of the gas molecules can be altered based on the configuration of the Buckybowl. Bowl up configurations tended to have larger binding energies than their bowl down counterparts which could be as much as half as strong. The type of Buckybowl also played a

role in the strength of binding. Sumanene interactions tended to be stronger than corannulene while coronene was generally the weakest where the interactions were largely driven by electrostatics and dispersion. Second, they found that attractive dispersion interactions play a major role in the binding of small molecules to Buckybowls. The dispersion component typically accounted for a majority of the attractive interaction which helped balance the Pauli repulsion. Additionally, bowl up systems had stronger dispersion and Pauli repulsion components which can be intuitively understood that the electronic wave functions between the adsorbate and adsorbent were in closer spatial proximity than in the bowl down state.

A computational study was performed by Armaković and coworkers on the adsorption properties of CO, $CO_2$, and $NH_3$ on sumanene [34]. Their thorough analysis made comparisons to adsorption on other carbon allotropes showing that adsorption energies with sumanene are generally equilvalent to or greater than (within 1 kcal/mol) carbon nanotubes, graphene, and $C_{60}$ fullerene. These adsorption characteristics help motivate investigations into Buckybowls for gas separation systems as they are predicted to perform well in gas adsorption. Furthermore, Armaković also investigated the nature of the interactions between gas molecules and sumanene and found that physisorption characteristics tend to dominate. Changes in frontier molecular orbitals were tracked by computing the density of states and comparing the changes between the adsorbed and non-adsorbed states. While molecules such as $NH_3$ did show characteristics of chemisorption through changes in the frontier orbitals, the interactions tended to stay non-covalent in nature.

Experiments have also been performed showing that sumanene can act as a gas adsorption system when arrayed on a surface. Jaafar *et al.* have shown that sumanene deposited on a Ag(111) surface can adsorb methane gas at low temperatures using a scanning tunneling microscope (STM) imaging [31]. Due to the curved nature of Buckybowls, they possess a dipole moment oriented from the outer edge of the bowl pointed towards the concave direction and located along the axis of the bowl. Electron density tends to be higher around the outer edge than within the bowl which creates a dipole. It was found that when sumanene is deposited on the Ag(111) surface, the orientation of the dipole plays a role in how the film of molecules is built up. For low coverage of sumanene on the surface, the molecules are typically found to be in the bowl up configuration while mixed patterns are found at higher

coverage. Interestingly, the bowls form a hexagonal pattern where the central molecule is in the bowl down state while the surrounding Buckybowls are bowl up. This effect is due to the energetic minimization of adjacent dipoles. Furthermore, Jaafar *et al.* also suggested that methane molecules preferentially bind to the bowl up Buckybowls with a single gas molecule oriented above the bowl. At higher methane concentrations the gas molecules were found to bind to the bowl down configurations as well with more coverage due to interactions with a larger surface area.

Finally, bowl inversion on a surface was addressed by Fujii and coworkers by utilizing an STM tip to lower the barrier to inversion on a Au(111) surface [32]. As with the Ag(111) surface, the bowl up configuration is preferred on Au(111) which was confirmed with simulated STM imaging. At room temperature they found the rate of switching (inversion) on the surface to be less than 0.005 Hz. As they brought an STM tip closer to the molecule, a critical distance was found which began influencing the rate of switching. Measurements of the current from the STM through the molecule were used to monitor the distance from the tip to the Buckybowl as well as its orientation. When the STM tip was at this critical distance they found that the switching rate significantly increased to 0.3-0.5 Hz as the energy barrier for the Buckybowl to adsorb to either the surface or STM tip was lowered.

These computational and experimental investigations provide evidence that Buckybowls are potential candidates for gas separation systems. The sensitivity of gas molecules to Buckybowls has been predicted computationally for a range of molecules and seen experimentally with methane. Selectivity among different molecules is predicted since each gas molecule has a different associated binding energy. Through significantly altered interaction energies due to the orientation of the Buckybowl, recycling is a possibility as gases can be adsorbed in the bowl up state and desorbed in the bowl down state under the right thermal conditions or due to an external force. Maximizing these three factors is key to creating a gas separation system which rivals the other main types. The first computational investigation in this thesis looks into small gas adsorption on Buckybowls with the aim of showing how the selectivity and sensitivity can be tuned by applying an external electric field. Novel interaction results for nitric oxide (NO) and nitrogen dioxide ($NO_2$) are presented in addition to controlled selectivity. Then the interaction energy for binding toxic molecules is calculated in an effort

to propose a system for capturing harmful gases. This thesis is concluded with thoughts on improving Buckybowls as gas separation systems through the use of functionalization and structures tailored to specific uses.

## 2.0 Theory

**It therefore becomes desirable that approximate practical methods of applying quantum mechanics should be developed, which can lead to an explanation of the main features of complex atomic systems without too much computation.**

***Paul Dirac***
*Quantum Mechanics of Many-Electron Systems, 1929*

The simplicity of performing electronic structure calculations on modern computational hardware belies the decades of often tedious work that went towards promoting our theoretical understanding of the chemistry of molecules and physics of materials. Prior to the advent of quantum mechanics, the fields of classical mechanics, electromagnetism, and their relativistic counterparts dominated our understanding of the universe. As is often mentioned in textbooks on the subject, this understanding was shattered by the solution to the ultraviolet catastrophe offered by Max Plank. Rather than acting as classical objects, energy transitions within molecules were recognized to be quantized. While this theory applied to vibrational transitions, shortly afterwards, the Bohr model was proposed stating that electronic transitions were also quantized [35].

This crucial insight blossomed into the fields of quantum physics and chemistry that form the basis of our current understanding of all chemical interactions. While the theory behind electronic wave functions was developed throughout the 1930's, algorithms necessary to solve the Schrödinger equation took many decades to refine. By 1935, Douglas Hartree had formulated his *ab intio* self-consistent field theory in a manner that was directly applicable to calculating atomic energy levels [36]. This method laid the foundation of mean-field theory with single particle wave functions existing within a potential generated by all of the other wave functions.

Before the advent of semiconductor-based computers, calculations using these methods took considerable time even for atomic systems. Simplifications were required to tackle electronic structure calculations on systems larger than diatomic molecules. John Pople's work enabled key improvements by defining two approximate methods, complete neglect of differential overlap and intermediate neglect of differential overlap [37, 38], in addition to compu-

tational method for efficiently calculating integrals over Gaussian basis functions [39, 40, 41] which were both key to granting researchers the ability to investigate larger systems . By 1973 the Pople group had released Gaussian70 to the chemistry community as computer technology started to improve [42]. Pople was awarded the Nobel Prize in Chemist in 1998 alongside Walter Kohn who both made significant contributions to the computational electronic structure community. Throughout the twentieth century, the underlying theory of quantum mechanics was harnessed through approaches which pushed the fields of chemistry and physics into the realm of computational tractability. This chapter focuses on elucidating the frameworks available to modern computationalists that have been employed in the research presented in the following chapters.

## 2.1 Density Functional Theory

*The following description of density functional theory is adapted from a previous work of the author, Density Functional Theory Study of Dilute Transition Metal Phthalocyanines* [43].

In a system described by quantum mechanics, understanding both the wave function and its energy eigenvalues is comparable to the classical mechanics description of finding the equation of motion and determining its solution. The time-independent Schrödinger equation provides a method of determining the wave function analytically for a few choices of external potential, while most other solutions must be tackled numerically. Early numerical solutions focused on using the Hartree-Fock method which posed the solution in the form of a Slater determinant[44]. In the 1960's Hohenberg, Kohn, and Sham formulated density functional theory (DFT) as a means to determine the properties of a system through the electron density rather than the wave function[45, 46]. While it may seem trivial that the properties would depend on the electron density, it was not clear that a knowledge of electron density was enough information to determine any ground state property which could also be determined by knowing the external potential. Essentially, Hohenberg, Kohn, and Sham showed that for any given external potential, there was a one-to-one mapping onto an electron density.

However, before a formulation of DFT is shown, first consider a system consisting of

nuclear cores and electrons. The Hamiltonian for such a system is:

$$H = \sum_{l} \left( \frac{-\hbar^2 \nabla_l^2}{2M} \right) + \frac{1}{2} \sum_{\substack{l,m \\ l \neq m}} \frac{Z^2 e^2}{|\boldsymbol{R}_l - \boldsymbol{R}_m|} + \sum_{i} \left( \frac{-\hbar^2 \nabla_i^2}{2m} \right) + \frac{1}{2} \sum_{\substack{i,j \\ i \neq j}} \frac{e^2}{|\boldsymbol{r}_i - \boldsymbol{r}_j|} - \sum_{i,l} \frac{Z e^2}{|\boldsymbol{r}_i - \boldsymbol{R}_l|} \quad (2.1)$$

where $M$, $Z$, and $\boldsymbol{R}$ are the nuclear mass, charge, and positions. The symbols $m$, $e$, and $\boldsymbol{r}$ refer to the equivalent electron quantities. Here the electron charge, $e$, is defined to be a negative value. The first and third terms refer to the kinetic energies of the nuclear charge and electrons. The second and fourth terms give the Coulomb interactions between the nuclear charges and electrons, respectively. The last term gives the Coulomb interaction of the electrons with the nuclear charges.

In this form, a solution to all but the most basic of problems would be near impossible with current computer hardware. Therefore, a few approximations can be applied to simplify this Hamiltonian. First, the Born-Oppenheimer approximation states that in the time scale relevant to electronic properties, the kinetic energy of the nuclear masses does not make a large contribution to the energy. Second, due to screening of the nuclear charges by the core electrons, the nuclear-nuclear interactions contribute relatively little. For the purposes of notational consistency with other authors, the electron-nuclear interaction can be approximated as the electrons interacting with an electric potential generated by all of the nuclear charges. Therefore, Eq. 2.1 reduces to:

$$H = \sum_{i} \left( \frac{-\hbar^2 \nabla_i^2}{2m} \right) + \frac{1}{2} \sum_{\substack{i,j \\ i \neq j}} \frac{e^2}{|\boldsymbol{r}_i - \boldsymbol{r}_j|} - \sum_{i} e V_{ext}(\boldsymbol{r}_i) \quad (2.2)$$

Despite the application of various approximations, this is still quite a formidable problem due to the book keeping of electron positions. If the number of degrees of freedom could be reduced, such as through a density function, the problem would be more approachable. Hohenberg and Kohn solved this problem through *Reductio ad absurdum* and the Rayleigh-Ritz variational principle.

To prove that each external potential maps to a unique density we will consider two different potentials, $V_1(\boldsymbol{r})$ and $V_2(\boldsymbol{r})$ which are assumed to give rise to the same charge density, $n(\boldsymbol{r})$. If we can disprove this assumption then we know that two arbitrary $V(\boldsymbol{r})$ cannot lead to the same $n(\boldsymbol{r})$; therefore, each $V(\boldsymbol{r})$ has a unique density associated with it. From the solution of the Schrödinger equation we know that the corresponding wave functions, $\psi_1(\boldsymbol{r})$ and $\psi_2(\boldsymbol{r})$, are different due to the difference in $V(\boldsymbol{r})$.

Using the Rayleigh-Ritz variational principle, Hohenberg and Kohn proposed that the energies of the two states satisfy the relation:

$$E_2 = \langle\psi_2|\, H_2\, |\psi_2\rangle < \langle\psi_1|\, H_2\, |\psi_1\rangle \tag{2.3}$$

which can be reformulated in terms of $H_1$ by considering the following change:

$$H_2 = H_1 - V_1(\boldsymbol{r}) + V_2(\boldsymbol{r}) \tag{2.4}$$

such that

$$E_2 < \langle\psi_1|\, H_1 - V_1(\boldsymbol{r}) + V_2(\boldsymbol{r})\, |\psi_1\rangle = E_1 + \langle\psi_1|\, V_2(\boldsymbol{r}) - V_1(\boldsymbol{r})\, |\psi_1\rangle \tag{2.5}$$

At this point it is useful to relate the charge density with the probability density $\psi^*\psi$. We will posit the following relation:

$$n(\boldsymbol{r}) = \sum_i n_i(\boldsymbol{r}) = \sum_i |\psi_i(\boldsymbol{r})|^2 \tag{2.6}$$

This relation allows us to rewrite Eq. 2.5 in terms of the density:

$$E_2 < E_1 + \int_V (V_2(\boldsymbol{r}) - V_1(\boldsymbol{r}))\, n(\boldsymbol{r}) d\boldsymbol{r} \tag{2.7}$$

If the converse situation is considered we find that:

$$E_1 < E_2 - \int (V_2(\boldsymbol{r}) - V_1(\boldsymbol{r}))\, n(\boldsymbol{r}) d\boldsymbol{r} \tag{2.8}$$

where the relation $n_1(\boldsymbol{r}) = n_2(\boldsymbol{r}) = n(\boldsymbol{r})$ was applied. Through the addition of Eqs. 2.7

and 2.8 a contradiction arises:

$$E_1 + E_2 < E_2 + E_1 \tag{2.9}$$

Therefore, the initial assumption is incorrect and it is true that each $V(\boldsymbol{r})$ has a uniquely defined $n(\boldsymbol{r})$. Now that we have shown that the potential due to the interactions with the ions in the system corresponds to a unique charge density we can formulate Eq. 2.2 in terms of this density.

Before this, however, it is useful to examine the Schrödinger equation resulting from Eq. 2.2 and digress into Hartree-Fock theory. Due to the interactions between each of the electrons in the Coulomb term the solution for the eigenstates is not straight forward and presents a considerable obstacle. Prior to the formulation of DFT the Hartree-Fock method was relied upon to generate solutions to a mean field version of the many-body Hamiltonian. This method defines a self-consistent procedure where the ground state of a system is found variationally.

The non-interacting wave function that the Hartree approximation leads to is a misnomer. In fact the electrons are interacting, it is only the dynamics of the system which is not captured in the calculation of the wave function for the single electron. The direct Coulomb interactions are replaced by a potential of the form shown in Eq. 2.10. This is equivalent to calculating the potential due to all of the other electrons, $j$, in the system and calculating the wave function of the electron at $i$. In reality the electrons of a system are all adjusting due to interactions with all of the other electrons, but this method utilizes the non-interacting approach by fixing all electrons except for a single electron solution.

$$V_i(\boldsymbol{r}_i) = \sum_{j \neq i} \frac{e^2 |\psi_j(\boldsymbol{r}_i)|^2}{\boldsymbol{r}_i - \boldsymbol{r}_j} d\boldsymbol{r}_j \tag{2.10}$$

Within the Hartree approximation the Schrödinger equation is resolved into a set of $N$ single electron equations where $N$ is the total number of electrons in the system. The total wave function is then found through the product state of all of the single electron wave functions. The self-consistent cycle to find the ground state solution is composed of the following steps:

1. Guess an initial wave function.
2. Compute Hartree potential
3. Solve the set of single electron equations
4. Populate occupied orbitals according to Aufbau and Hund's rules
5. Find the total wave function and calculate the energy.
6. Compare energies generated from initial guess and result. If energy difference is within tolerance then the ground state has been found. Otherwise, update the wave function and repeat the process.

In a sense, the requirement that the solution must be found self-consistently is a method of manually updating the non-interacting potential in place of the real, interacting picture.

An additional constraint is placed on the wave functions generated from this method by forcing all solutions to obey the Pauli exclusion principle. To reproduce the antisymmetric solutions Slater determinants are utilized where the elements are the single electron wave functions. As an example, a two electron system, such as $H_2$, the well known solution is:

$$\Psi\left(\boldsymbol{r}_1, \boldsymbol{r}_2\right) = \frac{1}{\sqrt{2}}\left(\psi_A\left(\boldsymbol{r}_1\right)\psi_B\left(\boldsymbol{r}_2\right) - \psi_B\left(\boldsymbol{r}_1\right)\psi_A\left(\boldsymbol{r}_2\right)\right) \tag{2.11}$$

where $\boldsymbol{r}$ accounts for both the spatial and spin variables. This can be written as a Slater determinant:

$$\Psi\left(\boldsymbol{r}_1, \boldsymbol{r}_2\right) = \frac{1}{\sqrt{2}}\begin{vmatrix} \psi_A\left(\boldsymbol{r}_1\right) & \psi_A\left(\boldsymbol{r}_2\right) \\ \psi_B\left(\boldsymbol{r}_1\right) & \psi_B\left(\boldsymbol{r}_2\right) \end{vmatrix} \tag{2.12}$$

The Hartree-Fock method is still in use today to understand the properties of atoms and molecules. Despite the power of such a method it still has a severe draw back when calculating electron-electron interaction. This failing is largely attributed to the absence of correlation effects in the Hartree Hamiltonian. DFT enters the picture again with its unique method of solving this shortcoming.

Following the groundbreaking work of Hohenberg and Kohn on the uniqueness of the charge density and form of the exchange-correlation functional, Kohn and Sham proposed

the following equation (aptly named the Kohn-Sham equation)[46]:

$$\left[\frac{-\hbar^2\nabla_i^2}{2m} - eV_{ext}\left(\boldsymbol{r}\right) + \int \frac{n_i\left(\boldsymbol{r}'\right)}{|\boldsymbol{r}-\boldsymbol{r}'|}d\boldsymbol{r}' + V_{xc}[n_i]\left(\boldsymbol{r}\right)\right]\psi_i\left(\boldsymbol{r}\right) = E_i\psi_i\left(\boldsymbol{r}\right) \tag{2.13}$$

which is a single-particle equation similar to the Hartree equation with the added $V_{xc}[n]\left(\boldsymbol{r}\right)$ exchange-correlation potential term which is a functional of the electron density and encapsulates all effects which are not accounted for in the other terms. Note that in the Hartree-Fock formalism the exchange is treated explicitly while correlation effects are neglected. It should also be noted that the kinetic term is the non-interacting kinetic term where the unknown interacting term is moved to $V_{xc}$. In theory, this should produce an exact solution of the system given that the correct form of $V_{xc}$ is known. However, this is not the case in practice as the exchange-correlation is approximated.

As shown by Hohenberg and Kohn through a variational technique, the energy for a system represented by the Hamiltonian in Eq. 2.13 is given by the expression [45, 46, 47]:

$$E[n] = T[n] + \int V_{ext}\left(\boldsymbol{r}\right)n\left(\boldsymbol{r}\right)d\boldsymbol{r} + \frac{1}{2}\int d\boldsymbol{r}\int d\boldsymbol{r}'\frac{n\left(\boldsymbol{r}'\right)n\left(\boldsymbol{r}\right)}{|\boldsymbol{r}-\boldsymbol{r}'|} + E_{xc}[n] \tag{2.14}$$

where $[n]$ denotes a quantity which is a functional of the density function, $V_{ext}$ is the system dependent potential due to the ionic positions, and $E_{xc}$ is the exchange correlation energy functional which incorporates all of the information not contained in the non-interacting scheme. The $E_{xc}$ is used to define $V_{xc}$ from Eq. 2.13 as shown in Eq. 2.15

$$V_{xc} = \frac{\delta E_{xc}[n]\left(\boldsymbol{r}\right)}{\delta n\left(\boldsymbol{r}\right)} \tag{2.15}$$

which states that $V_{xc}$ can be determined if we know the form of the variation of $E_{xc}$ with respect to the density. If $E_{xc}$ were known, we could use Eqs. 2.14 and 2.13 to solve for the Kohn-Sham eigenstates and eigenvalues of any system exactly. However, as previously stated, this is not the case as models and approximations are used to define $E_{xc}$.

Despite the limitation posed by a lack of knowledge of the form of $E_{xc}$ Eqs. 2.14, 2.13, and 2.6 define a set of equations which can be solved self-consistently similarly to the Hartree-Fock method. The difference is that an extra step is added to calculate the density from eigenfunctions of the Kohn-Sham equations. By minimizing the energy of the system with

respect to the density, a ground state density can be achieved within the limits of the chosen $E_{xc}$ functional.

## 2.2 Energy Decomposition Analysis

While understanding the electronic structure of single molecules provides insight into electronic transitions, many of the phenomena that we observe in nature are the results of interactions between molecules. These interactions can take many forms such as electrostatic which concerns the classical interactions between electronic orbitals and protons, or have a quantum nature such as Pauli repulsion or dispersion interactions between electrons. The most basic type of calculation to understand interactions is the supermolecular calculation. The interaction energy derived from this procedure for two interacting molecules follows from three separate calculations: One calculation for each molecule in vacuum and a third of the total system. The interaction energy, $E_{int}$, is then computed as,

$$E_{int} = E_{total} - (E_1 + E_2) \tag{2.16}$$

where $E_{total}$ corresponds to the energy of the total system while $E_1$ and $E_2$ are the separate energy calculations. Note that more negative values of $E_{int}$ yield stronger binding. In general, interactions do not have to be confined to those between two molecules. The interaction energy between groups of molecules can be computed in the same way. To standardize the nomenclature between these scenarios, I will use the term *fragment* to refer a group of atoms of which the user wishes to understand the interaction. For example, in the case of two interacting molecules, there are two fragments.

When performing calculations using a linear combination of atomic orbitals (LCAO) as the basis, the finiteness of the basis set introduces its own form of error. Known as basis set superposition error (BSSE), this error stems from the utilization of basis functions between fragments in the complex system. Suppose the interaction energy is computed according to Eq. 2.16 above using a LCAO basis. For a two-fragment system, three energies are computed: The energy of the complex and the energies of the isolated fragments. During

the SCF calculation of the complex, basis functions from one fragment can use the basis functions located on the other fragment to minimize the energy. This results in a situation where the basis functions on each fragment in the complex are effectively larger than their isolated counterparts. Therefore, a strict subtraction of the energies is not a one-to-one comparison. BSSE can be accounted for using a counterpoise correction as suggested by Boys and Bernardi[48]. By calculating the energy of a fragment in the basis of the complex, $E_{1,cmplx}$, the error introduced by BSSE is,

$$E_{BSSE} = E_{1,cmplx} - E_1 \tag{2.17}$$

which must be calculated for each fragment. Subtracting this quantity from Eq. 2.16 yields the counterpoise corrected interaction energy.

Total interaction energies are composed of several components which makes it necessary to define a formalism that allows a researcher to break down the contributions to the interaction energy. One such method is that proposed by Kitaura and Morokuma in 1976 (KM method) [49]. Their strategy for decomposition revolved around the use of single fragment molecular orbitals (MOs) to partition the total MO space. Consider the Hamiltonian for an interacting system,

$$H = H_A + H_B + H_{AB} \tag{2.18}$$

where $A$ and $B$ are fragments and $AB$ represents the total system. Now, suppose that as the basis for the total system (furthermore, referred to as the *complex*), $\psi$, we use the fragment MOs,

$$\psi_i = \sum_k C_{ik}\phi_{A,k} + \sum_\mu C_{i\mu}\phi_{B,\mu} \tag{2.19}$$

where the $\phi$ are orbitals in the fragments. Using this basis, the unperturbed energy would be,

$$E_0 = \langle A_0 | H_A | A_0 \rangle + \langle B_0 | B_A | B_0 \rangle \tag{2.20}$$

where $|A_0\rangle$ and $|B_0\rangle$ represent the orbitals in the fragment basis. The Hartree-Fock method can then be employed to calculate the complex MOs subject to constraints which define each component of the interaction energy. The KM method breaks this down into the electrostatic, polarization, exchange, and charge transfer interactions. Electrostatic terms consist of the occupied orbitals which interact among themselves. Polarization is defined as the interaction present from mixing between the occupied and vacant orbitals on a single fragment. Exchange is the interaction between the occupied orbitals of the fragments from exchanging electrons. Charge transfer is the relaxation of orbitals between fragments and is composed of the occupied orbitals from one fragment interacting with the vacant orbitals of the other fragment. Despite its wide applicability, the KM method suffers from numerical instabilities and interpretation problems.

With a wide range of energy decomposition methods (EDA methods) to choose from, the following will present two important modern methods. The first, symmetry adapted perturbation theory (SAPT) was one the first EDA methods to be developed and, as the name suggests, is derived from applying perturbation theory to the interaction. Then the absolutely localized molecular orbital (ALMO) method is briefly described. Note that these two methods represent fundamentally different approaches to the same problem. Whereas SAPT requires a perturbative treatment assuming that the interaction energy is a small contribution to the total energy, ALMO focuses on a variational treatment where orbitals are optimized by applying component driven constraints and minimizing the energy.

### 2.2.1 Symmetry Adapted Perturbation Theory

Symmetry adapted perturbation theory (SAPT) is a method used to separate out the contributions to the interaction energy, $E_{int}$, between interacting fragments using perturbation theory. Similar to the KM method described above, first and second order components broadly take the form of the electrostatic, exchange, induction, and dispersion contributions. The basis behind this theory has a long history rooted in applying the Rayleigh-Schrödinger perturbation theory (RSPT) method to understanding interactions which have an energy

scale much smaller than the energies of either fragments,

$$E_{int} \ll E_A + E_B \tag{2.21}$$

where we are will consider a system of two fragments, $A$ and $B$.

Intuitively, as two fragments are brought together from an infinite distance, the orbitals begin to have stronger interactions. These interactions manifest in altered orbital distributions which is known as polarization. This led to the precursor to SAPT - *polarization theory*. Following the description of Jeziorski *et al.* [50], polarization theory begins with the simple RSPT assumption of the time-independent Schrödinger equation,

$$(H_0 + \lambda V) |\Psi_{AB}\rangle = E_{AB} |\Psi_{AB}\rangle \tag{2.22}$$

where $H_0$ is the fragment Hamiltonian $H_0 = H_A + H_A$, $\lambda$ is the perturbation parameter, $V$ is the perturbative operator, $\Psi_{AB}$ is the wave function of the complex, and $E_{AB}$ is the energy of the complex. Here, complex refers to the total system including all interactions. As a simple test, we see that when $\lambda = 0$ the equation reverts to the sum of the contributions from each fragment separately,

$$E_{AB}(\lambda = 0) = E_A + E_B = E_0$$
$$\Psi_{AB}(\lambda = 0) = \Psi_A \Psi_B = \Psi_0$$

Note here we are defining the zeroth order parameters $E_0$ and $\Psi_0$.

Defining the interaction energy, $E_{int}$, as,

$$E_{int} = E_{AB} - E_0 \tag{2.23}$$

we can expand the complex wave function and interaction,

$$\Psi_{AB}(\lambda) = \sum_{n=0}^{\infty} \lambda^n \Psi_{pol}^{(n)} \tag{2.24}$$

$$E_{int} = \sum_{n=1}^{\infty} \lambda^n E_{pol}^{(n)} \tag{2.25}$$

where we have defined the polarization components to be the higher order terms which are affected by the interaction between the fragments. Note that while $\Psi_{AB}(\lambda)$ includes all expansion terms, the interaction energy starts at $n = 1$ since $n = 0$ is explicitly removed from the definition.

An expression for the interaction energy in terms of the complex wave functions can be derived by computing the energy terms of Eq. 2.22,

$$\begin{aligned} \langle\Psi_0|\left(H_0 + \lambda V\right)|\Psi_{AB}\rangle &= E_{AB}\langle\Psi_0|\,|\Psi_{AB}\rangle \\ \implies E_0\langle\Psi_0|\,|\Psi_{AB}\rangle + \langle\Psi_0|\,\lambda V\,|\Psi_{AB}\rangle &= E_{AB}\langle\Psi_0|\,|\Psi_{AB}\rangle \\ \implies E_0 + \langle\Psi_0|\,\lambda V\,|\Psi_{AB}\rangle &= E_{AB} \end{aligned} \tag{2.26}$$

where we have defined the phase relation,

$$\langle\Psi_0|\Psi_{AB}\rangle = 1 \tag{2.27}$$

Therefore, the interaction energy can also be written as,

$$E_{int} = \langle\Psi_0|\,\lambda V\,|\Psi_{AB}\rangle \tag{2.28}$$

Substitution the polarization relations into Eq. 2.28 yields,

$$\sum_{n=1}^{\infty} \lambda^n E_{pol}^{(n)} = \langle\Psi_0|\,\lambda V\left(\sum_{n=0}^{\infty} \lambda^n \left|\Psi_{pol}^{(n)}\right\rangle\right) \tag{2.29}$$

and collecting similar terms in $\lambda$ we can determine the polarization energy at an arbitrary order,

$$
\begin{aligned}
E_{pol}^{(1)} &= \langle \Psi_0 |\, V \,| \Psi_0 \rangle \\
E_{pol}^{(2)} &= \langle \Psi_0 | V | \Psi_{pol}^{(1)} \rangle \\
&\vdots \\
E_{pol}^{(n)} &= \langle \Psi_0 | V | \Psi_{pol}^{(n-1)} \rangle
\end{aligned}
$$

where the relation $\Psi_0 = \Psi_{pol}^{(0)}$ was used. While this expression is analytically correct, in practice the higher order terms could not be computed without the corresponding polarization wave functions. Hirschfelder *et al.* provide a solution to this problem in the form of a recurrence relation [51],

$$
\Psi_{pol}^{(n)} = -\hat{R}_0 V \Psi_{pol}^{n-1} + \sum_{k=1}^{n-1} E_{pol}^{(k)} \hat{R}_0 \Psi_{pol}^{(n-k)} \tag{2.30}
$$

where the resolvent operator, $\hat{R}_0$, is defined as,

$$
\hat{R}_0 = \sum_{m \neq 0} \frac{|\Psi_m\rangle \langle \Psi_m|}{E_m - E_0} \tag{2.31}
$$

where the sum is over excitations of the ground state $\Psi_0$.

These relations now allow us to investigate the contributions of the various corrections to the interaction energy. Let's consider corrections up to second order,

$$
E_{int} \approx E_{pol}^{(1)} + E_{pol}^{(2)} \tag{2.32}
$$

As stated above, the first-order correction can be written as,

$$
E_{pol}^{(1)} = \langle \Psi_0 |\, V \,| \Psi_0 \rangle \tag{2.33}
$$

which can be explicitly written in terms of the charge densities of the fragments by noting that $V$ is the Coulomb operator acting between fragments,

$$
E_{pol}^{(1)} = \int \int d\boldsymbol{r_1} d\boldsymbol{r_2} \rho_A(\boldsymbol{r_1}) \frac{1}{r_{12}} \rho_B(\boldsymbol{r_2}) \tag{2.34}
$$

where the integrals are over all of real space, $\rho_A$ is the charge density on fragment A, and $r_{12} = |\boldsymbol{r_1} - \boldsymbol{r_2}|$. Note that this expression includes nuclear contributions to the charge density such that,

$$\rho(\boldsymbol{r}) = \sum_{\alpha} Z_\alpha \delta(\boldsymbol{r} - \boldsymbol{R_\alpha}) - \rho'(\boldsymbol{r}) \tag{2.35}$$

where the sum is over all nuclei belonging to the fragment, $Z$ is the atomic number of the atom, $R$ is the position of the nuclei, and $\rho'(\boldsymbol{r})$ is the electronic contribution to the charge density. Therefore, based on classical physics, we see that the first-order contribution derives from the electrostatic interactions between the fragments.

At second order we find,

$$\begin{aligned} E^{(2)}_{pol} &= \langle \Psi_0 | \, V \left| \Psi^{(1)}_{pol} \right\rangle = \langle \Psi_0 | \left( -\hat{R}_0 V \left| \Psi^{(0)}_{pol} \right\rangle \right) \\ &= - \langle \Psi_0 | \, V \hat{R}_0 V \, | \Psi_0 \rangle = - \sum_{m \neq 0} \frac{| \langle \Psi_0 | \, V \, | \Psi_m \rangle |^2}{E_m - E_0} \end{aligned}$$

where it is important to note that the sum run over excited states. Traditionally, this terms is partitioned into two parts. Since the interaction is regarded as a small contribution to the complex energy, the orbitals also remain roughly similar to the unperturbed orbitals. With this understanding, an excited orbital can be stated in a couple of different ways. First, one form of excitation is to excite an electron on a single fragment which leaving the orbitals on the other fragment in the initial state. This type of interaction is known as the *induction energy* because it describes how the occupied orbitals from one fragment cause excitations on the other fragment. The second form of excitation is to consider excited states located on both fragments. This quantum effect describes the correlated nature of the instantaneous motion of the electrons. Instantaneous multipole moments are generated and cause an attractive force between fragments known as *dispersion*.

From second-order polarization theory we have derived three quantities: electrostatics, induction, and dispersion which contribute to the interaction energy between fragments. However, one serious failing of this method is its treatment of the fermionic nature of the wave functions. With standard RSPT the antisymmetric nature of the orbitals cannot be

represented leading to an inaccurate description of the exchange interaction between electrons. This problem is solved with the use of *weak symmetry forcing* which directly includes an antisymmeterization operator (Asymm) in the calculation of the interaction energy,

$$E_{int} = \frac{\langle \Psi_0 | \, V\mathcal{A} \, | \Psi_{AB} \rangle}{\langle \Psi_0 | \, \mathcal{A} \, | \Psi_{AB} \rangle} \tag{2.36}$$

where the Asymm operator, $\mathcal{A}$, has been added to include only those components of the wave function which contribute to its fermionic nature. Note that the same perturbation treatment from polarization theory is applied with the added ingredient of $\mathcal{A}$ in the energy expansion. This ultimately leads to exchange terms to be generated when calculating the different orders of the interaction energy,

$$\begin{aligned} E_{pol}^{(1)} &= E_{ES} + E_{Ex} \\ E_{pol}^{(2)} &= E_{Ind} + E_{Ind-Ex} + E_{Disp} + E_{Disp-Ex} \end{aligned}$$

where $E_{ES}$ is the electrostatic energy, $E_{Ind}$ is the induction component, and $E_{Disp}$ represents the dispersion term. When discussing the components of SAPT EDA, the exchange terms are typically included with their respective components except for the electrostatics. For example, the induction component is composed of both $E_{Ind}$ and $E_{Ind-Ex}$.

While SAPT is typically lauded as the gold standard of energy decomposition, in practice the calculations can take a significant amount of resources to perform. Historically, calculations proceeded in two steps with Hartree-Fock describing the zeroth order terms and more accurate methods such as MPn or coupled cluster to describe correlation. Density functional theory can be employed with the SAPT formalism in a method known as SAPT-DFT, but several drawbacks are also present here. Most notably is the inability of DFT to accurately describe dispersion interactions which are corrected by including time consuming time dependent DFT calculations to compute excitations. In addition to the high cost of calculation, SAPT is fundamentally unable to handle strongly interacting systems due to the nature of perturbation theory unless multiconfiguration methods are employed. Beyond SAPT, other methods have been developed to increase computational efficiency or introduce

more interpretable energy contributions or strong interactions. One such method is based on localizing molecular orbitals to fragments and will be discussed in the following section.

### 2.2.2 Absolutely Localized Molecular Orbitals

The absolutely localized molecular orbital (ALMO) method shares many features with the KM method as described above [52]. Most notably, contributions to the interaction energy are derived from restrictions placed on the atomic orbital (AO) to molecular orbital (MO) transition. Rather than define all of the terms in one step though, the ALMO method employs a series of self-consistent steps to build up the components of the interaction. Before explaining each of these steps it is important to note that the framework of the self-consistent field (SCF) optimization is fundamentally different than a normal SCF method. ALMO employs the self-consistent field - molecule interaction (SCFMI) formalism in order to generate properly antisymmetrized wave functions from fragment contributions. If the reader is interested in understanding what this entails, it is suggested to look at the work of Gianinetti *et al.* [53] and Nagata *et al.* [54] for more information.

ALMO separates the interaction energy components into the frozen, polarization, and charge transfer contributions. Technically, geometric distortions should be included within the interaction energy, but for the current purposes this will be assumed to be negligible because it can be calculated simply from the change in energy between the isolated fragment and complex structures. The first component, the frozen energy, is defined as the energy due to the fragments interacting without any optimization of the orbitals,

$$E_{Frozen} = E(\Psi_0) - \sum_x E(\Psi_x) \tag{2.37}$$

where $\Psi_0$ represents the complex orbitals where no relaxation of the orbitals has taken place, the sum is over all of the fragments in the complex, and $\Psi_x$ is the fully optimized wave function for each isolated fragment. An intuitive picture of this type of interaction is that this is the energy that results simply from moving the fragments close to each other from infinitely far away.

The next step encompasses the polarization component. Now that the fragments are

placed into their positions in the complex, the orbitals can be relaxed with the restriction that no charge transfer is allowed. This means that the MO coefficient matrix is block diagonal such that orbitals from one fragment cannot utilize the orbitals on another fragment. The polarization contribution can be expressed as,

$$E_{Pol} = E(\Psi_{SCFMI}) - E(\Psi_0) \tag{2.38}$$

where the SCFMI procedure is employed for the constrained orbital optimization. It is important to note that the polarization energy defined here is not the same as from the polarization method as described in the section on SAPT. While they are conceptually similar, SAPT polarization is defined as an alteration to the MOs of one fragment due to other MOs on the same fragment in addition to the the MOs of another fragment regardless of the contribution. ALMO, on the other hand, considers this term to be a component defined by changes to the MOs on one fragment due to MOs on another.

Finally, charge transfer can be computed as the difference between the polarization energy and full SCF optimization,

$$E_{CT} = E(\Psi) - E(\Psi_{SCFMI}) \tag{2.39}$$

where $\Psi$ is the full, optimized wave function for the complex. With the intuitive understanding of orbitals existing on various fragments, atomic basis functions are best suited for ALMO. However, as is known for calculating interaction energies, basis set superposition error is encountered when the orbitals from one fragment utilize the orbitals on other fragments during the complex calculation. Essentially this means that the effective basis sets for the complex are different than was used in the single fragment calculations and the energies are not comparable without some correction. To alleviate this problem in ALMO, the counter-poise correction is made during the charge transfer step since it includes the full SCF calculation.

In the preceding section I have attempted to give a general overview of two of the most important methods utilized by the energy decomposition community. SAPT is typically considered the gold-standard for calculating interaction energies, but it suffers from high

computational cost. ALMO attempts to alleviate some of these problems by utilizing Kohn-Sham orbitals and partitioning the energy into a few interpretable components. However, there are still drawbacks to using ALMO such as ambiguous terms resulting from overlap of basis sets between fragments, breaking down the frozen energy into more meaningful contributions, as well as the limitations of density functional theory on which the method is based. Many of these problems have been recently addressed in a more advanced ALMO method presented by Paul Horn and coworkers [55] which is utilized in the calculations performed in the following chapters.

## 3.0 Small Gas Molecule Adsorption on Buckybowls

> **We shall presume that this type of force, which is not conditioned by the existence of a permanent dipole or any higher multipoles, will be responsible for the Van der Waals attraction of the rare gases and also of the simple molecules $H_2$, $N_2$, etc. For reasons which will be explained presently these forces are called the *dispersion effect.***
>
> ***Fritz London***
> *The General Theory of Molecular Forces, 1936*

*The following work is part of a manuscript to be submitted. I would like to thank Dr. Keith Werling for his helpful contributions with constrained geometry optimizations. All other work is my own.*

Concentrations of carbon dioxide and methane in the atmosphere have increased 20.2% and 12.9%, respectively, since recording began in the early 1980's by the National Oceanic and Atmospheric Administration. [56, 57] These two molecules, produced primarily as a byproduct of burning fossil fuels, natural processes, and livestock [58], have been identified as significant green houses gases due to their ability to absorb and re-emit infrared radiation from the surface back towards Earth. Similarly, nitric oxide (NO) and nitrogen dioxide ($NO_2$) are produced from burning fossil fuels, are toxic to humans, and contribute to chemical processes which create ozone. [58, 59] Areas of heavy industry or transportation congestion are impacted by the smog produced from NO, $NO_2$, and $O_3$ causing increased occurrence of respiratory illness. [60] While $CH_4$, $CO_2$, NO, and $NO_2$ are necessary components of a healthy atmosphere, the regulation of these gases is critical to reducing their adverse impacts when present in excessive quantities.

Various technologies have been developed for separating gases such as membrane filtration [61, 62, 63], cryogenic distillation [63], absorption [63, 64], and adsorption [63, 65]. Recent advances in adsorption technologies show potential for tuning selectivity based on surface chemistry. [65] For instance, Guo *et al.* investigated the use of electric fields to tune the adsorption properties of several gas molecules on a *h*-BN surface and showed that the strength of the field can be used to induce stronger binding in a reversible interaction with $CO_2$. [66] Carbon-based capture technologies have also been used for gas capture in the form

of carbon nanotubes [67, 68, 69, 70] and doped graphene sheets [71, 72, 73, 74]. Recently, investigations into gas adsorption have been performed on Buckybowls which are molecules derived from the bowls of a Buckyball using a planar cut. [75, 31, 34, 76, 77, 33] Due to the structure of the Buckybowls, they offer a promising mechanism for both gas capture and release by controlling the depth of the bowl via an external electric field.

This study investigates the ability of coronene, corannulene, and sumanene to act as a capture and release molecule with respect to the atmospheric gases listed previously. In particular, this work quantifies the adsorption interactions of $CH_4$, $CO_2$, NO, and $NO_2$ under an applied electric field. The bowls undergo structural deformation that causes the depth to change due to the electric field. This change in bowl depth alters the adsorption properties such that the selectivity can be tuned for specific gases. Electric fields between -20 and +20 V/nm are applied and the adsorbate-adsorbent interaction is studied through an energy decomposition analysis (EDA).

This paper is outlined as follows: The computational approach of calculating the interaction energies ($E_{int}$), energy decomposition, and molecular dynamics are explained. Findings are then presented in the Results and Discussion section which is split into two parts. First, the zero field interactions are explained followed by the EDA with an applied electric field for all cases. The conclusion summarizes the findings and gives insight into further avenues of exploration for Buckybowls.

### 3.1 Computational Approach

The quantum chemistry package QChem [78] was employed to explore the non-covalent adsorbent-adsorbate interactions under the influence of an electric field. Adsorbates were paired with each adsorbent in configurations including both the bowl up (BU) and bowl down (BD) states. This resulted in twenty systems total due to the planar symmetry of coronene. Each systems was optimized at the $\omega$B97X-D/pc-1 level of theory. Electric fields from -20 to +20 $V/nm$ were chosen at 0.2 $V/nm$ increments. To simulate the effect of the adsorbent attached to a surface, rotations were projected out of the Hessian during optimization under

the influence of an electric field. This fixed the field to be parallel to the bowl inversion direction.

Optimized structures were then used to calculate the energy decomposition analysis (EDA) using an absolutely localized molecular orbital approach at the $\omega$B97M-V/pc-2 level of theory. It is important to note that the choice of functional was influenced by the $\omega$B97 series' ability to adequately describe non-covalent interactions. Furthermore, $\omega$B97M-V is a range-separated non-local functional which is of the type required for the specific EDA method used in this study along with Hartee-Fock chosen as the dispersionless functional used in calculating the dispersion and Pauli repulsion. The polarization consistent basis sets were chosen for their clear path to improve accuracy and performance in non-covalent systems when paired with the $\omega$B97 functionals.

Bowl depths are computed for all structures as the vertical distance between carbons in the central ring and those in the outermost ring. As the bowl depth changes so too does the interaction between the adsorbent and adsorbate. The density overlap region indicator (DORI) was chosen as as method to visualize the interaction as it elucidates regions of non-covalent interactions through changes in the electron density [79]. The total DORI interaction is computed by taking the integral over all space of the DORI densities with a value of 0.5 or greater.

## 3.2 Results and Discussion

An ideal gas capture device displays high sensitivity and selectivity towards a particular adsorbate. In the cases studied here, these qualities are encapsulated in the interaction energy between a Buckybowl and gas molecule. Sensitivity is governed by the strength of $E_{int}$ while differences between the energies yield selectivity. An external electric field is applied to the system to alter the binding properties on the Buckybowls which in turn causes the values of $E_{int}$ to change. Each adsorbate interacts with the Buckybowls differently resulting in ordering changes between the interaction energies. These differences are explored using the EDA method mentioned previously.

### 3.2.1 Adsorbate Orientations at Zero Field

While the structures of $CH_4$ and $CO_2$ binding to Buckybowls have been reported previously [33, 34], the results for NO and $NO_2$ are novel which are shown in Figure 3. The profile and top-down views are provided for each configuration. Starting with coronene there are a few features that are worth noting. Methane binds to the surface with three hydrogen atoms directed downward while the central carbon atom is located above one of the carbons located along the central ring of coronene. $CO_2$ is orientated horizontally with the oxygen atoms positioned above the central ring and one of the outer rings. Similar to $CO_2$, both NO and $NO_2$ are also oriented horizontally. The energetic minimum for NO straddles a C-C bond which forms the boundary between the central and outer rings with the oxygen atom closer to the center of coronene. $NO_2$ follows suit with its oxygen atoms located above a central and outer ring. The nitrogen atom straddles the C-C bond located between the rings.

The structures with corannulene are complicated by the addition of two systems for each adsorbate due to the bowl orientation. The most noticeable aspect of the geometries is that the adsorbates orient themselves so as to follow the contour of the bowl. The linear molecules $CO_2$ and NO illustrate this phenomenon the best. For both the BU and BD cases, $CO_2$ is oriented at an angle over the side of the bowl. In the BD case the carbon atom sits above the center of an outer ring with the oxygen atoms pointing outward radially. The BU case is slight different with the carbon atom positioned above a central carbon atom. The $CH_4$ molecule's orientation also conforms to the shape of the bowl. In the BD state methane is located above an outer ring and angled such that the three hydrogen atoms pointing towards the bowl are at the angle of the bowl. The BU case simply has the methane molecule located directly over the central ring. NO is similar to $CO_2$ is that the angle radially follows the contour of the bowl. In the BD configuration, NO is located over an out ring with the nitrogen atom positioned directly above the space with the oxygen atom pointing radially outward. The BU configuration is similar except the adsorbate is located over the central ring with the nitrogen atom at the center. Finally, $NO_2$ is particularly interesting because of its orientation. In the BD state, the oxygen atoms are pointing towards the bowl and are positioned over two C-C bonds at the walls of the rings. The oxygen atoms are pointed

away from the bowl in the BU state with the nitrogen atom placed over a C-C bond in the central ring wall.

Some structures of the sumanene systems are quite similar to corannulene with a couple significant exceptions. First, a minor difference in methane occurs in the BD case where the $CH_4$ is located above the central ring as opposed to an outer ring. The positioning of $CO_2$ and NO is nearly identical to the corannulene cases and needs further description. The orientation of $NO_2$ however, shows a clear difference. In the BD configuration the oxygen atoms point away from the bowl instead of towards it as in the corannulene case. The BU state for this system is similar to what is found in corannulene.

### 3.2.2 Trends in Binding Energies Between Adsorbates and Buckybowls

Similar to previous studies, adsorption to Buckybowls was found to be stronger in the BU configuration for all adsorbates as shown in Table 1. [33, 34]. In general, the interaction energies for S(BU) are the largest followed by C(BU) (about 2-3 times larger than the BD configurations) and then coronene. Interestingly, $CH_4$ and $CO_2$ binding to S(BD) are stronger than C(BD), but this trend is reversed for NO and $NO_2$. Note that the interaction energies for NO and $NO_2$ on coronene are calculated using supermolecular energies with couterpoise correction in contrast to the other values which are calculated with the EDA2 method.

### 3.2.3 Binding Energy Trends Within Applied Electric Fields

**3.2.3.1 Sumanene** At zero field in the sumanene BD configuration, $CO_2$ has the strongest interaction energy followed by $NO_2$ and NO which are nearly the same, and $CH_4$ with the weakest binding as shown in Figure 4. As a positive electric field is applied, $CO_2$ remains the most strongly bound until 6 V/nm where the interaction energy of $NO_2$ becomes comparable. The interaction energy of these two adsorbates initially weakens and then begins to strengthen around 6 V/nm. $CH_4$ becomes more strongly bound as a positive electric field is applied while NO only becomes weaker. A crossover between $CH_4$ and NO occurs around 6 V/nm as NO becomes the most weakly bound adsorbate. This behavior suggests that

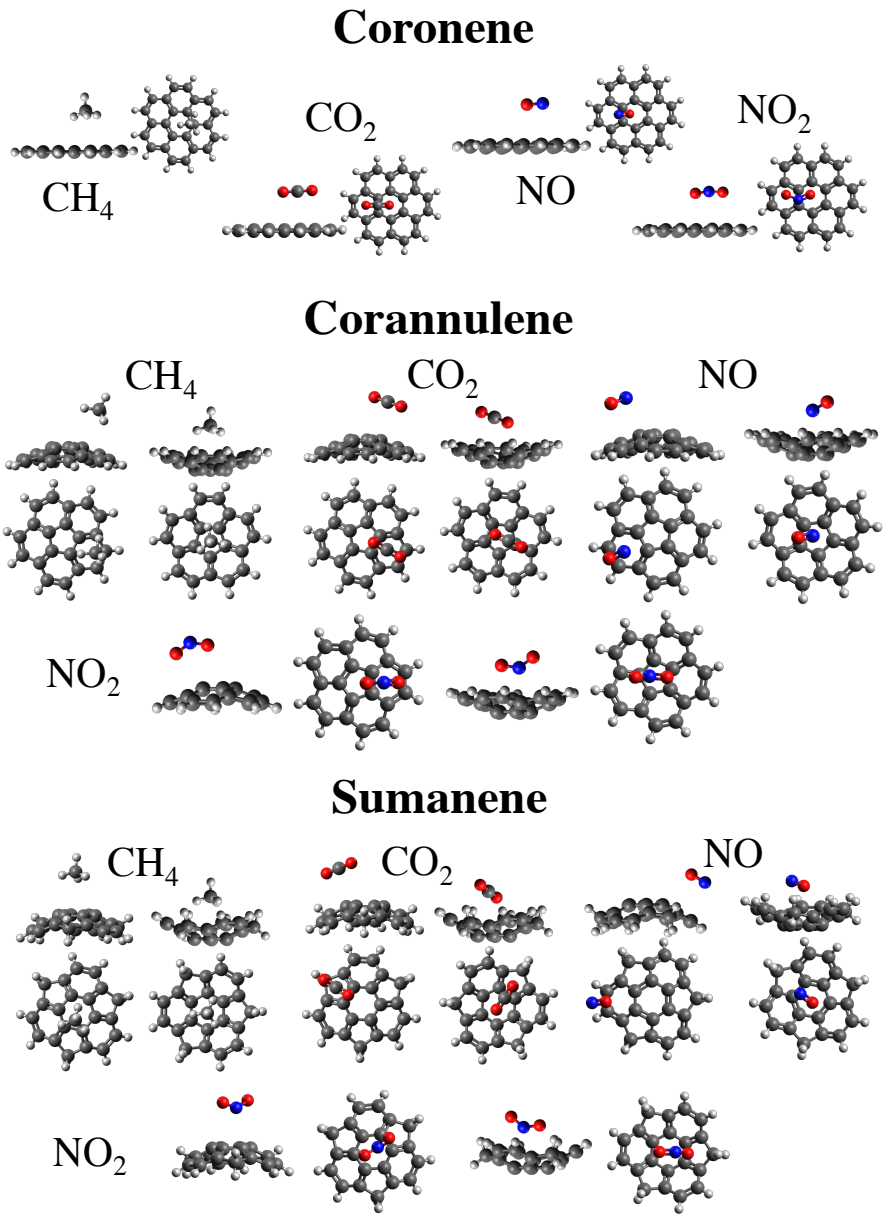


Figure 3: Optimized geometries and binding energies for all adsorbates on coronene (R), corannulene (C), and sumanene (S). Results are calculated using $\omega$B97X-D/pc-1//$\omega$B97M-V/pc-2 level with energy decomposition analysis including counterpoise corrections. Blue indicates nitrogen while red is oxygen.

| Molecule | $CH_4$ | $CO_2$ | $NO_2$ | NO |
|---|---|---|---|---|
| Sumanene (BU) | -5.56 | -6.11 | -6.04 | -4.34 |
| Sumanene (BD) | -1.82 | -3.29 | -2.33 | -1.40 |
| Corannulene (BU) | -4.82 | -4.77 | -5.19 | -3.93 |
| Corannulene (BD) | -1.73 | -2.96 | -2.35 | -2.08 |
| Coronene | -2.95 | -3.71 | -3.43[a)] | -2.38[a)] |

Table 1: Interaction energies in kcal/mol at the ωB97M-V/pc-2 level of theory within the EDA2 approach. [a)] The EDA2 method for NO and $NO_2$ on coronene failed to converge. Therefore supermolecular interaction energies as obtained at the ωB97M-V/pc-2 level of theory with BSSE corrections are presented.

positive electric field can be used to adjust the selectivity of sumanene since the ordering of the binding strength changes. On the other hand, binding becomes stronger across all adsorbates when a negative field is applied. The ordering from zero field is preserved until -8 V/nm when NO becomes the most

The ordering of the strength of the binding at zero field in the BU orientation is NO < $CH_4$ < $NO_2$ < $CO_2$ with $NO_2$ and $CO_2$ having comparable binding strengths. NO is the most weakly bound adsorbate and remains so until 14 V/nm on the positive side and -16 V/nm with a negative field. It is remarkable to note that over the range of -12 to 16 V/nm the total interaction energy of NO remains almost constant in contrast to the behavior exhibited by other adsorbates.

$CH_4$ displays a nearly linear relationship between the applied field and interaction energy. At negative fields, the binding becomes stronger by 2.71 kcal/mol while weakening by 2.05 kcal/mol with a positive field. $CO_2$ follows similar behavior with smaller changes in interaction energy for positive fields. $NO_2$ changes the most dramatically with a 2.93 kcal/mol decrease in binding strength with positive applied fields and a 3.31 kcal/mol increase in strength with a negative applied field.

Due to the change in interaction energy of $NO_2$, the ordering of the binding strengths

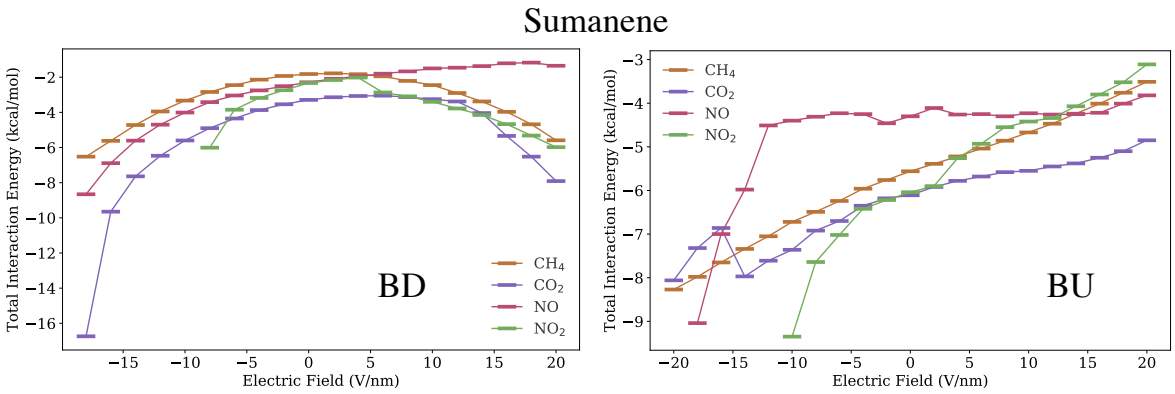


Figure 4: Interactions energies of adsorbates on sumanene as a function of electric field. Bowl down (BD) orientation is shown on the left and bowl up (BU) on the right.

change as the field changes. At positive fields $NO_2$ becomes more weakly bound than $CH_4$ so the ordering changes to NO < $NO_2$ < $CH_4$ < $CO_2$. With negative applied fields, $NO_2$ becomes the most strongly bound at -2 V/nm and the ordering changes to NO < $CH_4$ < $CO_2$ < $NO_2$.

**3.2.3.2 Corannulene** At zero field in the corannulene BD configuration, the ordering of binding strengths is $CH_4$ < NO < $NO_2$ < $CO_2$ which is shown in Figure 5. With positive applied fields, the interaction energies of $NO_2$ stay nearly the same with small variations. Similarly, the binding of $CH_4$ remains nearly constant and becoming slightly more strongly bound at 14 V/nm. $NO_2$ becomes slightly more strongly bound as positive fields are applied while the binding of $CO_2$ initially weakens and then becomes slightly stronger. The ordering at positive fields changes to NO < $CH_4$ < $CO_2$ < $NO_2$ at 10 V/nm but the differences in interaction energy are small between NO and $CH_4$ (0.25 kcal/mol) as well as $CO_2$ and $NO_2$ (0.02 kcal/mol). More dramatic changes in interaction energy occur at negative fields where the binding strength increases for each adsorbate. An ordering change occurs at -8 V/nm where $NO_2$ becomes more strongly bound than $CO_2$ ($CH_4$ < NO < $CO_2$ < $NO_2$).

In general for the BU systems, interaction strengths become slightly weaker with positive

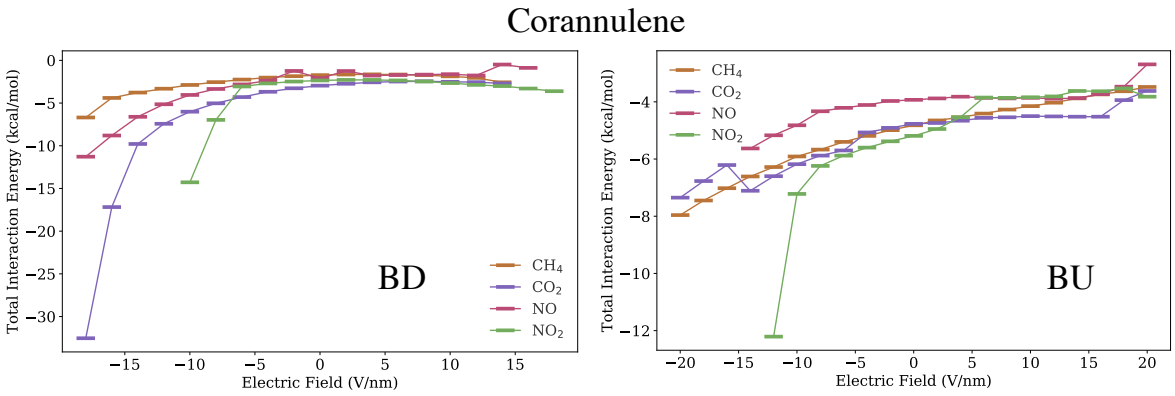


Figure 5: Interactions energies of adsorbates on corannulene as a function of electric field. Bowl down (BD) orientation is shown on the left and bowl up (BU) on the right.

fields while becoming stronger at negative fields. Both NO and $CO_2$ exhibit only slight changes in interaction energy at positive fields with $NO_2$ changing the most dramatically. The ordering at zero field (NO < $CO_2$ < $CH_4$ < $NO_2$) is not preserved as it changes to NO < $CH_4$ < $CO_2$ < $NO_2$ at 2 V/nm, NO < $CH_4$ ≈ $NO_2$ < $CO_2$ at 4 V/nm, and then to $NO_2$ < NO < $CH_4$ < $CO_2$ at 6 V/nm. $NO_2$ changes from being the most strongly bound to the weakest over the course of a 6 V/nm change indicating that the selectivity of $NO_2$ can be altered using an applied electric field. At negative electric fields a change in the ordering occurs at -6 V/nm (NO < $CH_4$ < $CO_2$ < $NO_2$) where $CO_2$ becomes more strongly bound than $CH_4$.

**3.2.3.3 Coronene** Similarly to the BU cases with the Buckybowls, NO has the weakest interaction energy initially for coronene as shown in Figure 6. This trend is preserved at positive fields while a switch in the ordering occurs at -10 V/nm where $CH_4$ becomes a weaker binding molecule. The binding energy of $NO_2$ becomes nearly equivalent to $CH_4$ at positive fields and shows the same behavior of the binding becoming slightly stronger. At negative fields, $NO_2$ begins to strongly bind and becomes the strongest at -8 V/nm until it dissociates after -10 V/nm. Overall, the interactions energies either do not change (NO) or

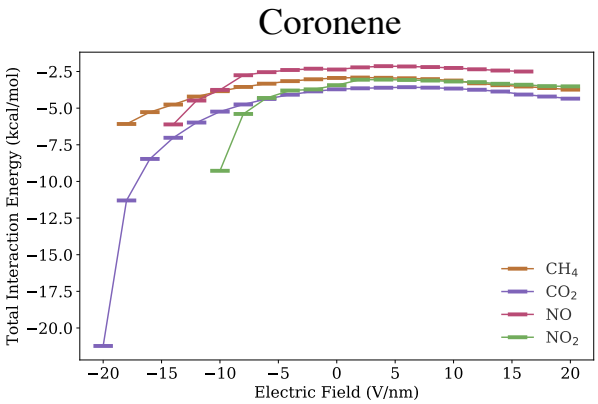


Figure 6: Interactions energies of adsorbates on coronene as a function of electric field. Bowl down (BD) orientation is shown on the left and bowl up (BU) on the right.

become slightly more bound with positive fields where the coronene molecule begins to bend in the BU orientation. Negative fields induce a more precipitous change in the interaction energy as the molecule bends away from the adsorbate in a BD orientation.

### 3.2.4 Energy Decomposition Analysis

To elucidate the binding mechanism between the adsorbates and the different molecules, we performed energy decomposition analysis. Intuitively, there are two main modes of non-covalent interactions with Buckybowls: electrostatics and dispersion. Buckybowls possess dipole moment due to the anisotropic distribution of electron density along the bowl axis. Compared to the planar coronene, excess electron density is found of the outer edge of the bowl creating an electric dipole moment oriented from the bottom of the bowl pointing towards the open end. Being composed of sections of Buckyballs, Buckybowls possess numerous aromatic carbon rings which contribute to dispersion interactions. The curvature of the bowls leads to increased interactions with the conjugated $\pi$-orbitals inside of the bowl compared to the outside.

Hussain *et al.* examined non-covalent interactions in coronene, corannulene, and sumanene

with $CH_4$ and $CO_2$ adsorbates. [33] They performed an LMO energy decomposition analysis of the interaction energy and found that the interactions were largely influenced by the attractive dispersion force and Pauli repulsion. The magnitudes of these components varied between the bowl up (BU) and bowl down (BD) orientations such that the interactions in the BU case were generally stronger in agreement with the results reported in the previous section.

**3.2.4.1 Sumanene** As previously mentioned, Figure 4 indicated that an external electric field alters the interaction energy of the systems such that the ordering of strengths is changed. NO and $NO_2$ display clear ordering changes for both the BD and BU cases. In the BD system, positive fields cause the binding of the two adsorbates to behave differently. While the interaction strength of NO decreases, $NO_2$ shows an increase in strength. Figure 7 presents the EDA for all of the systems to help elucidate the cause for this difference. First, at zero field, the binding between the two adsorbates arises from two different mechanisms. While NO is charge transfer bound, the interaction with $NO_2$ is largely driven by the frozen interaction terms with small contributions from polarization and charge transfer. As the field strength is increased the frozen contribution of NO becomes weaker until it begins to be repulsive. Coupled with only a slight increase in the charge transfer component, the total interaction energy becomes weaker. On the other hand, both the frozen and charge transfer components contribute to a stronger interaction with $NO_2$ as the field strength is increased. At negative fields both NO and $NO_2$ show stronger interaction strengths, with $NO_2$ being stronger until it desorbs after -8 V/nm.

The binding of methane in the BD configuration is largely driven by frozen interactions for small field strengths. While the interaction energy becomes stronger as the strength of the field increases, different mechanisms begin to dominate between positive and negative fields. At negative fields the frozen component remains dominant while at positive fields charge transfer becomes stronger and contributes significantly to the interaction energy by 20 V/nm. Negative fields drive the interaction energy to become stronger for $CO_2$ in the BD orientation. At first, this is driven by an increasing contribution from the frozen component but charge transfer and polarization begin to take over by -16 V/nm. At positive fields the

interaction energy stay roughly similar until about 14 V/nm where the interaction strength grows due to the frozen contribution.

In the BU configuration, the interaction energy for NO remains fairly constant until a strong negative electric field is applied. At positive fields, we see from Fig. 7 the EDA components are not significantly altered by the strength of the field. However, with negative fields the composition of the interaction begins to change. Whereas the interaction was dominated by the frozen component at zero field, the charge transfer component begins to strengthen and thus compensating for a weaker frozen component. After -10 V/nm the charge transfer component dominates and leads to a significantly stronger interaction energy. $NO_2$ in this configuration exhibits a simple interaction trend of strengthening for negative fields and weakening for positive fields. At zero field the interaction is dominated by the frozen component which largely drives the changes in the interaction energy. The charge transfer component becomes more apparent at stronger negative fields until desorption occurs after -10 V/nm. The polarization component strengthens slightly for positive fields, but can not compensate for a reduction in the frozen component leading to weaker total interaction energies.

Interestingly, interaction energies for $CH_4$ in the BU state follow a linear trend with field strength. The strength increases at negative fields while it decreases for positive fields. This trend is largely driven by the frozen component until at high positive fields where charge transfer becomes significant. Similarly for $CO_2$, a near linear dependence on the electric field is observed. Positive fields see weaker interaction strengths whereas stronger interactions are found with negative fields. In contrast to $CH_4$ the frozen component is the major contributor across all electric fields. Sharp changes of the interaction strengths are found a field strengths lower than -14 V/nm. The frozen interaction changes at these fields driven by a change in bonding characteristics and structural modification.

**3.2.4.2 Corannulene** Interaction energies for corannulene show similar trends as those found in the sumanene-based systems with the distinction that the interactions are generally weaker. In the BD configurations, NO and $NO_2$ have similar interaction energies at positive fields with only minor changes as the strength increases before a bowl inversion occurs.

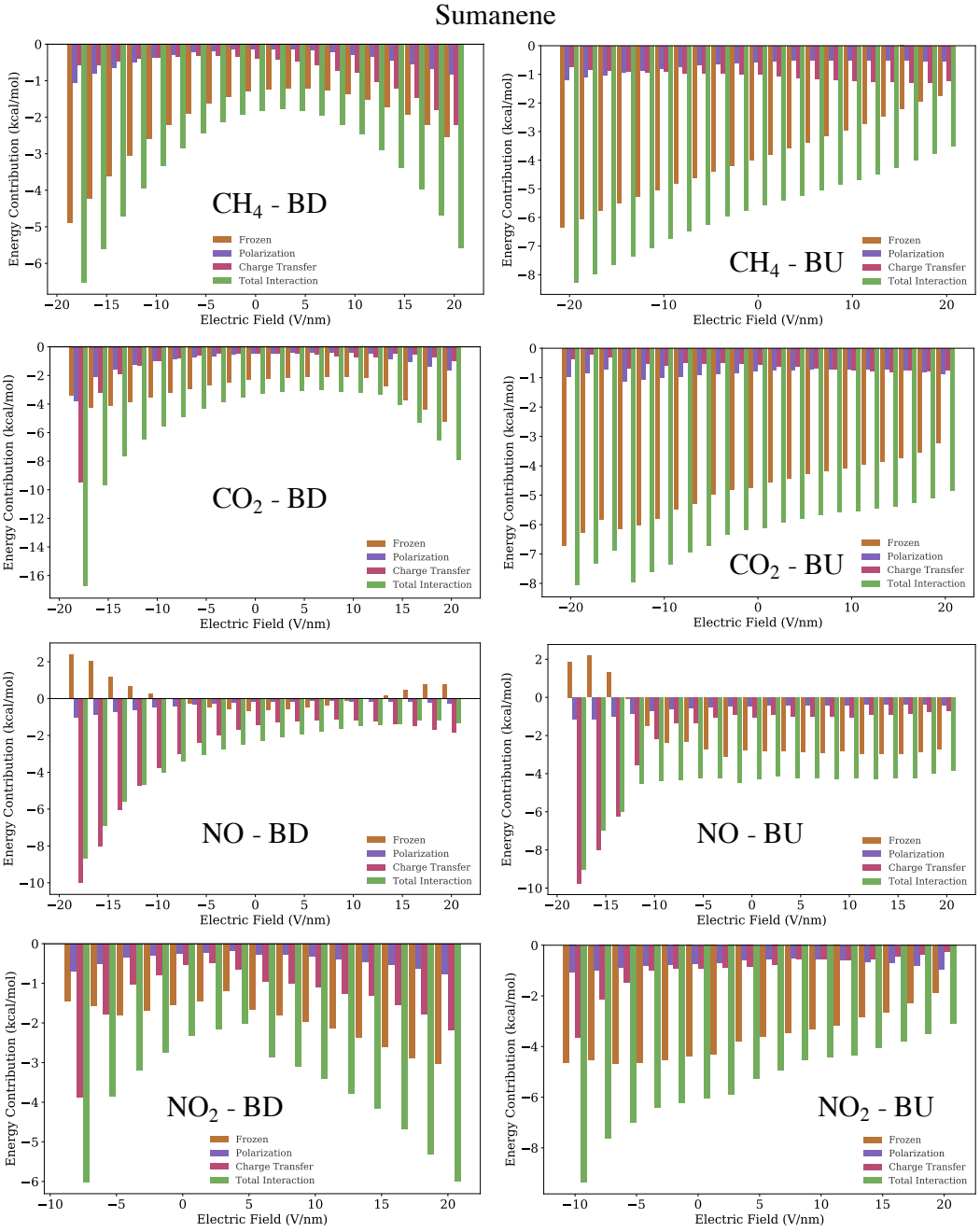


Figure 7: Energy decomposition analysis for adsorbates on sumanene in the bowl down (BD) and bowl up (BU) configurations.

Despite these similarities, Figure 8 indicates that the nature of the interactions are quite different. The interaction energy for NO is largely dominated by the charge transfer energy whereas $NO_2$ has a combination of frozen and charge transfer components. At negative fields, the two interaction energies diverge with $NO_2$ becoming significantly stronger until desorption occurs at -10 V/nm with a significant charge transfer contribution. The charge transfer components of NO become steadily stronger, overcoming the repulsive frozen component contributions.

Interaction energies for the $CH_4$-BD system increase in strength at negative fields which is due to an associated growing contribution from the frozen component. This change is also accompanied by an increase in the charge transfer and polarization components adding to the interaction energy. At positive fields the interaction energy remains nearly unchanged until about 8 V/nm where the interaction energy begins to strengthen again. Note that the positive field strength only scales to 14 V/nm because after this point the corannulene inverts causing the $CH_4$ to lose its binding. At positive fields the interaction energies of $CO_2$ remain relatively unchanged with little variation in the components of the interaction. However, at negative fields the interaction energy becomes considerably stronger. This trend follows an increase in the charge transfer and then the polarization component at the most negative fields. After -14 V/nm the strength of the frozen component begins to decrease sharply and becomes repulsive. This trend is indicative of the $CO_2$ a chemical bond forming between the adsorbate and adsorbent. Structurally, this is accompanied by a bend in the O-C-O bond.

As shown in Fig. 5, the interaction energies for NO and $NO_2$ have similar values following 6 V/nm in the BU configuration, despite the strength of $NO_2$ binding being stronger than NO by about 1.5 kcal/mol at zero field. The interaction energy of NO does not change much over this range and the EDA as shown in Fig. 8 indicates that the components largely do no change except for a reduction of charge transfer and frozen components after 16 V/nm. Similarly, the components of $NO_2$ do not change considerably except for a decrease of the charge transfer and frozen components contributing to the sharp change around 6 V/nm. At negative fields, both systems become more strongly bound due to changes in the charge transfer and polarization component that overcome the reduction of the frozen energy.

The interaction energies for $CH_4$-BU follow a nearly linear trend in a similar fashion as

the sumanene system. At negative fields the interaction energy becomes stronger due to a steady increase in the contribution from the frozen component. The interaction energy becomes weaker with positive fields driven by a reduction in the frozen component. Note that the charge transfer contribution begins to increase at higher fields causing the rate of change of the interaction energy to decrease. With $CO_2$ as an adsorbate, the frozen component dominates the interaction. The strength of the interaction energy increases at negative fields except for fields lower than -14 V/nm where there interaction energy weakens due to a drop in the frozen, polarization, and charge transfer components. At positive fields up to 16 V/nm the interaction energy stays steady with the various contributions not changing much. At fields larger than that the interaction energy decreases due to a reduction in the frozen energy contribution which is slightly countered by an increase in polarization.

**3.2.4.3 Coronene** Figure 9 shows the EDA results for $CH_4$ and $CO_2$ on coronene. Interaction energies for $CH_4$ follow similar trends as those found in the corannulene $CH_4$-BD system. Negative electric fields increase the strenth of the interaction through the frozen contribution and slight changes in the charge transfer and polarization. Small positive fields have little effect on the interaction energy until after 6 V/nm where the strength begins to grow. Despite this increasing strength, the frozen contribution becomes weaker while. Stronger binding is due to an increased influence from charge transfer in this case.

The interaction energy of $CO_2$ binding to coronene with an applied positive electric field becomes slightly stronger. Since there is little change to the polarization and charge transfer components, this increase is driven by changes in the frozen contribution. At negative electric fields the situtation changes dramatically as the interaction energy becomes considerably stronger at fields below about -10 V/nm. As the total interaction strength increases, the frozen component remains fairly constant even becoming weaker at -20 V/nm. The largest factor in the change comes from a significant increase in the contribution from the charge transfer component and to a lesser extent the polarization.

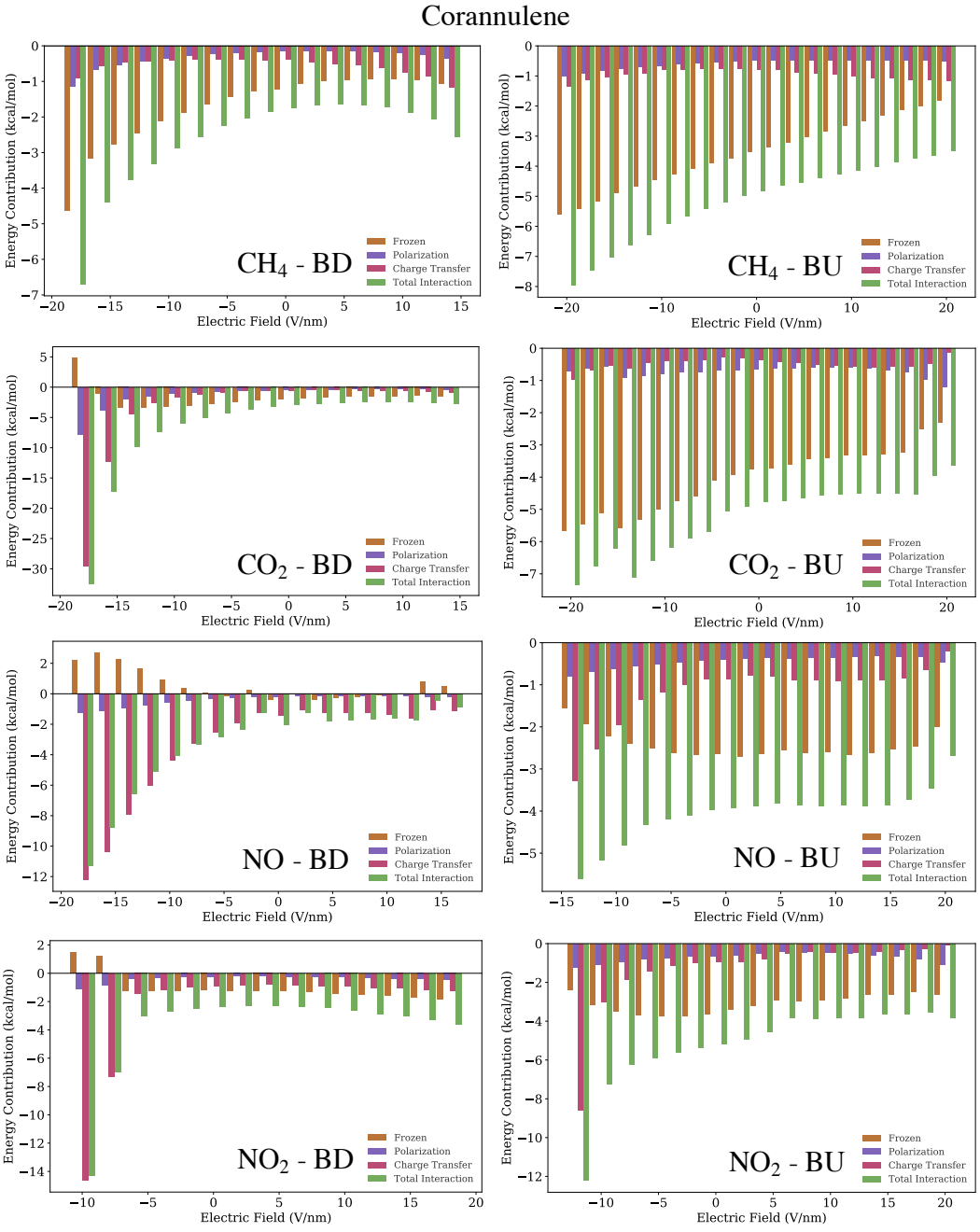


Figure 8: Energy decomposition analysis for adsorbates on corannulene in the bowl down (BD) and bowl up (BU) configurations.

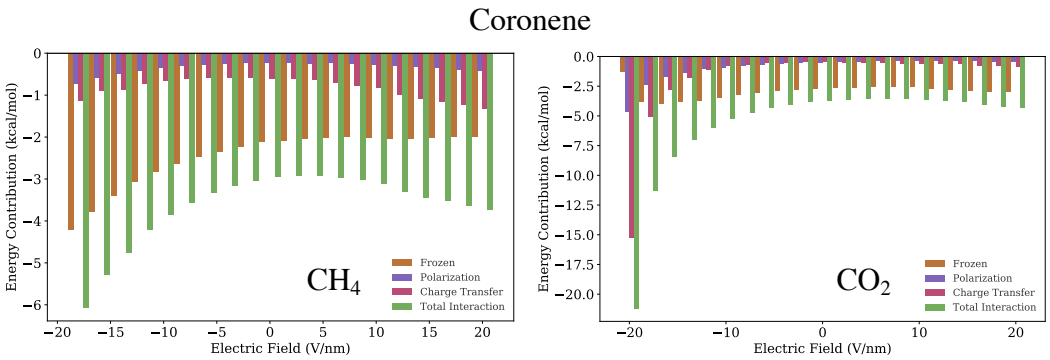


Figure 9: Energy decomposition analysis for adsorbates on coronene in the bowl down (BD) and bowl up (BU) configurations.

### 3.2.5 Bowl Depth and DORI

Buckybowls naturally possess a dipole moment due to the asymmetric distribution of electron density along the bowl axis. The outer side of the bowl will tend to have a higher electron density than the inside which generates a dipole pointing from the convex to convave portions on the molecule. Under an applied electric field, the electron density adjusts to minimize the energy of interaction. For instance, consider a Buckybowl in the BU state with a positive applied electric field. The electron density will adjust such that the convex side becomes more negative while the concave side becomes more positive - a strengthening of the dipole. Associated with this change is a rearrangement of the nuclei to minimize the stress due to the altered electron density. Ultimately this interaction would lead to a larger bowl depth. All of these changes contribute to differences in interaction energies which were presented in the previous section.

In theory, the changes of the interaction energy should be evident from the integrated DORI values for each of these systems. Figure 10 shows the integrated DORI and bowl depth values for all of the sumanene systems as an external electric field is applied along the bowl axis. For the BD state we see that the bowl depth decreases as a positive electric field is applied as expected because charge density is rearranged such that the electronic density

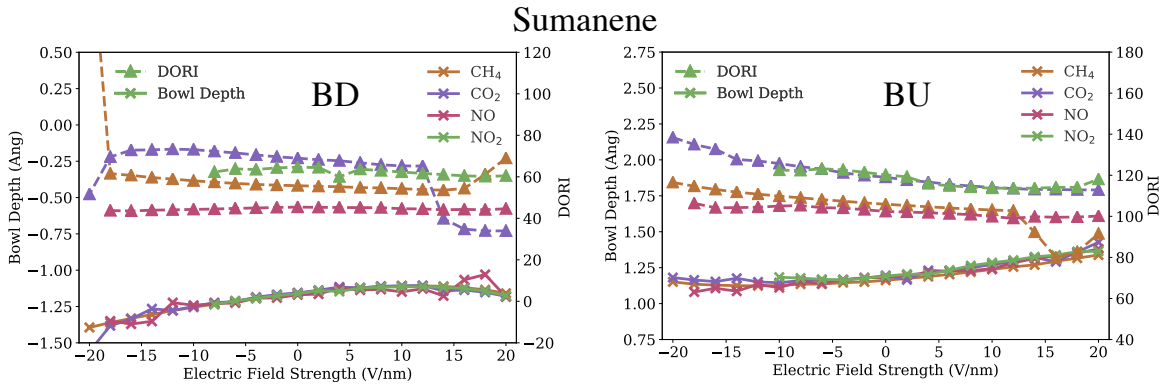


Figure 10: Bowl depth and integrated density overlap regions indicator for sumanene systems. Note that DORI values shown in the figure are calculated from the difference of spatially integrated DORI values of the fragments from the complex.

along the convex side must decrease while a growing bowl depth is found for negative fields. Note that negative bowl depths are recorded for the BD states because the difference is measured from the carbon atoms forming the central ring to those along the outer ring. Therefore, a shallower bowl depth would be progressing towards a flat molecule. The DORI values on the other hand become more complicated to analyze. Across all adsorbates, the DORI values do not change much at small field strengths and only show significant variation once the strength of the field becomes larger. A strong decrease in integrated DORI is recorded at high field strengths for $CO_2$ which corresponds with a sudden change in the frozen component of the interaction as shown above. The BU case follows similar trends with a sharp decrease in DORI value for $CH_4$, but this is not correlated with any significant change from the interaction energy indicating that while the electron density overlap changes appreciably, the interaction energy does not depend heavily on this change. Bowl depth follows the expected trend of increasing at positive fields and decreasing for negative fields.

Similar to the sumanene case, Figure 11 shows the bowl depth and DORI for all corannulene systems. The bowl depths for both the BD and BU systems have the same expected trends as sumanene indicating that the same mechanism of charge redistribution causing

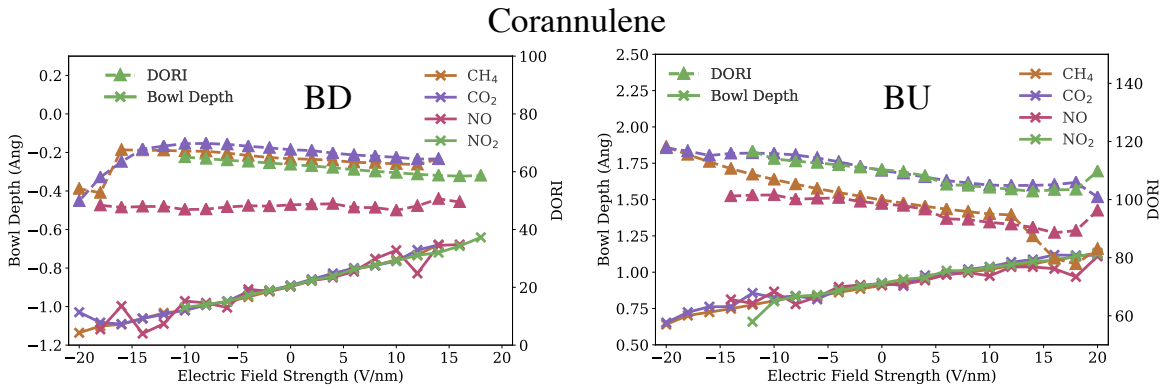


Figure 11: Bowl depth and integrated density overlap region indicator for corannulene systems. Note that DORI values shown in the figure are calculated from the difference of spatially integrated DORI values of the fragments from the complex.

bowl depth change is seen. Overall, the DORI values follow the same trend too. At least at small field strengths, the DORI values decrease going from negative to positive fields. A few points are worth noting however. In the BD case, $CO_2$ undergoes a decrease in DORI at negative fields which is accompanied by an increase of interaction energy due to charge transfer. Together these trends indicate that the charge transfer determined from the EDA is based on density overlap between the adsorbate and adsorbent. While there are dips in the DORI for $CH_4$ and NO in the BU configuration, there are no accompanying shifts in the interaction energy components indicating that while the density overlap is changing, there is no correlation to a response of the interaction energy.

Finally, Figure 12 shows the bowl depths and integrated DORI for the coronene systems. In contrast to the corannulene and sumanene cases, an increase in the DORI is observed going from negative to positive fields. This coincides with a change in bowl depth. At negative fields coronene deforms such that it assumes a BD configuration while positive fields yield a BU structure. The integrated DORI remains nearly constant across all fields except for a dip after 14 V/nm which occurs when the charge transfer component establishes a larger contribution to the total interaction energy. The sharp rise at -20 V/nm can be considered

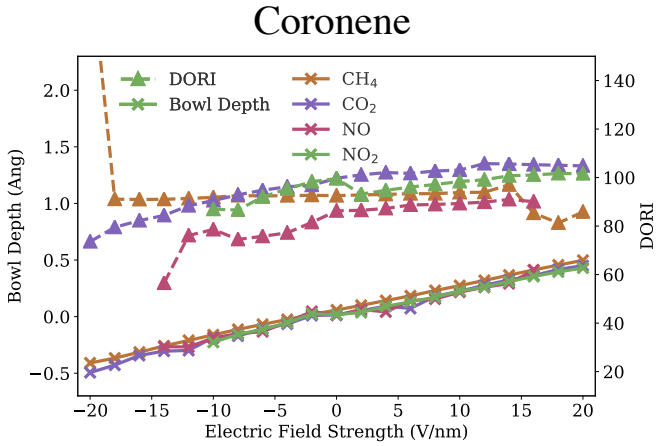


Figure 12: Bowl depth and integrated density overlap regions indicator for coronene systems. Note that DORI values shown in the figure are calculated from the difference of spatially integrated DORI values of the fragments from the complex.

anomalous because charge population analysis indicates that an electron transfers from the coronene to $CH_4$ and begins the desorption process.

Overall, the picture to draw from these results is that while the integrated DORI is known to be a good benchmark for interaction, strict correlations are not always forthcoming. Significant trends in the DORI sometimes correspond to changes of the interaction energy at points where the component's composition begins to change, but it is difficult to draw a concrete conclusion. In the future, it might be helpful to correlate spatial changes in the DORI with clear differences of the components of the interaction energy.

### 3.3 Conclusion

Nano-engineered devices are changing many industries through creating devices specifically tailored to a particular application. The field of gas capture/release is no exception with current research on engineered MOFS, zeolites, and carbon-based capture systems.

Buckybowls offer another route to creating engineered devices by tuning interactions with adsorbates through the application of an external electric field. Buckybowls occur in a range of sizes which offer varied strengths of interaction. Here, we showed that the bowl-up configurations of sumanene and corannulene showed the largest interaction strength while the bowl-down states were the lowest. Coronene results were provided as a middle ground between the bowl-up and bowl-down states and had interaction energies between the bowl-up and bowl-down values.

We presented interaction energies and the associated energy decomposition analysis for $CH_4$, $CO_2$, NO, and $NO_2$ to aid in identifying novel systems for capturing green house gases and atmospheric pollutants. In particular, NO and $NO_2$ adsorption on Buckybowls has not been previously reported in literature as far as the authors are aware. Structurally, each system relaxed in the electric field resulting in either a deeper or flatter bowl depth. The change in structure and electronic polarization produced altered interaction energies with respect to the zero-field values. This phenomenon opens the possibility of devices composed of Buckybowls to be used as sensitive gas capture/release devices where the strength of the electric field controls the strength of interaction.

Finally, our results indicate that these systems possess selectivity through changing the order of the strengths of the interaction energies under an applied electric field. The ability to remove components of a gas mixture is a desired property of gas capture/release devices and our results indicate that Buckybowls would be appropriate for experimental studies into this effect.

## 4.0 Sumanene as an Adsorbent for Upper Respiratory Tract Irritants

> **If it were not so, if we were organisms so sensitive that a single atom, or even a few atoms, could make a perceptible impression on our senses - Heavens, what would life be like!**
>
> ***Erwin Schrödinger***
> *What is Life, 1944*

Threshold limit values (TLVs) are set by the Occupational Health and Safety Administration (OSHA) to define the safe concentration of a chemical to which workers are exposed during the normal conduct of their jobs. These limit values can be set by comparing data from animal experiments and human interactions to give industrial companies a guideline to follow for their employees. Research into the effects of gases on the respiratory system have been of interest since the development of gas warfare during the first world war and has seen continued interest ever since. Following the second world war, industrial gas exposure became a primary concern as workers were now exposed to a wide variety of chemical compounds with little understanding of how new chemicals would affect the human respiratory system. For instance human exposure to oil fogs was investigated by Lushbaugh *et al.* by understanding the effects on animals [80].

In the late 1960's and early 1970's Yves Alarie at the University of Pittsburgh proposed the $RD_{50}$ metric to standardize how we measure respiratory irritation [81]. His work laid the foundation for using data from animal experiments to inform TLV generation for compounds which human exposure was too dangerous. By the 1990's a database of $RD_{50}$ values had been compiled for a wide range of chemicals [82]. As animal testing becomes more undesirable, numerical experiments replace live animal studies and the reliance on this compiled database becomes critical to providing a basis of our understanding of the effect chemical compounds on our respiratory tract.

The three most potent chemicals found in this database are 2-chlorobenzalmalonitrile (CS, $RD_{50}$=0.42 ppm), 1,6 hexamtheylene diisocyanate (HDI, $RD_{50}$=0.17 ppm), and toluene diisocyanate (TDI, $RD_{50}$=0.2 ppm). In 1928, Ben Corson and Roger Stoughton developed a respiratory irritant that is widely used today [83]. Known as CS gas (labeled CS above)

after the researchers, this compound has become a primary irritant used in tear gas by police forces and militaries around the world. At room temperature this chemical remains in solid form so deployment often includes aerosolizing a powder or vaporizing through the use of heat. A few studies have been performed for the detection of CS gas as its detection is an important component in some criminal investigations [84, 85].

Even more potent are the to diisocyanate compounds HDI and the more widely used TDI which are used in industrial coatings and the manufacture of polyurethane. These chemicals possess properties which are highly desirable in the coating industry such as high tolerance of abrasion and inactivity towards ultraviolet light. In spite of their extraordinary applications, these compounds represent significant hazards as respiratory irritants and must be protected against.

As described in Chapter 3, gas separation processes are useful tools to remove unwanted compounds from a gas stream through a variety of different methods. In particular, Buckybowls are proposed as adsorbents for capturing small gas molecules in a capture/release system driven by the two possible states of the bowl - bowl down (BD) or bowl up (BU). It was shown that small gas molecules adsorbed to the Buckybowls with different interaction energies based on the configuration and the details of the interaction were investigated via energy decomposition analysis. In this chapter, the three compounds of interest: CS, HDI, and TDI will be studied computationally in a similar fashion. While no external electric fields will be employed in the calculations, the goal is to determine the strength of the interaction, identify the components of the interaction which are dominant, and to discover any barriers to adsorption due to possible geometric changes.

## 4.1 Computational Details

All computations were carried out using the Q-Chem 5.0 quantum chemistry package [78]. Optimizations were performed at the $\omega$B97X-D level of theory, which includes the Grimme dispersion correction, with a pc-1 double zeta basis set. Numerous structural configurations were explored during the optimization to make sure that the structures found were as close

to global minima as reasonably possible. Energy decomposition analyis was run using the EDA2 method as described by Horn *et al.* [55] at the optimum structures with a $\omega$B97M-V/pc-2 level of theory which includes non-local correlation as implemented in the VV10 functional to account for dispersion interactions [86].

The freezing string method (FSM) was employed as implemented in Q-Chem to determine if transition barriers exist due to geometric changes during the adsorption process [87]. In this method, transition paths are interpolated along the potential energy surface (PES) connecting the product and reactant. Nodes are chosen at both ends and extended along tangents to the reaction path. Structures at each node are optimized with the constraint that only changes perpendicular to the path are allowed. This process ends when the nodes meet on the PES. Six computations of the gradient were performed at each node with a step size equivalent to 15 initial nodes between the product and reactant structures. These values were chosen as the optimum relation between accuracy and time for generating accurate reaction paths at the same level of theory as the geometry optimizations.

## 4.2 Results & Discussion

The three respiratory irritants that were chosen for this study are shown in Figure 13 along with their associated $RD_{50}$ values [82]. CS shown on the left is distinguished by the chlorobenzene molecule with a malononitrile functional group. In the center, HDI is shown with the isocyanate groups placed at the ends of the carbon chain hexamethylene. Lastly, on the right is TDI which contains an isocyanate group at the 2 and 4 positions of toluene. The $RD_{50}$ values are reported in a concentration of part per million (ppm) which shows that HDI is the most potent followed by TDI and CS.

### 4.2.1 Geometric Distortions

Due to its Buckybowl nature, sumanene has two configurations for adsorption: bowl down (BD) and bowl up (BU). Figure 14 shows the optimized structures for all systems.

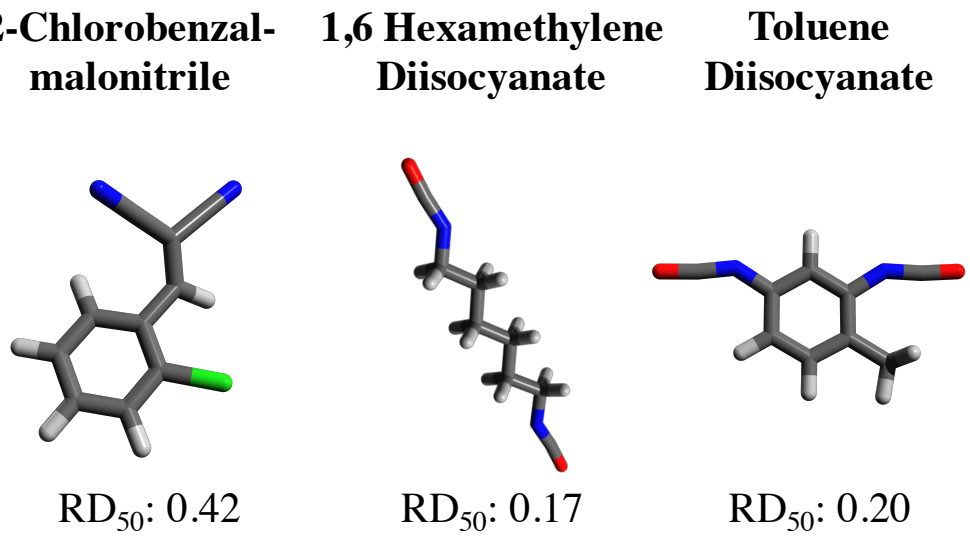


Figure 13: Potent respiratory irritants from Scahper and Alarie database. These molecules represent the most potent compounds which have been tested on animal subjects. The $RD_{50}$ (ppm) value of these molecules was determined as the concentration at which the respiratory rate of the mice was decreased by half (**R**espiratory **D**ecrease 50). Carbon atoms are colored gray, nitrogen are blue, oxygen is red, and chlorine is green. Hydrogen atoms are white.

Each adsorbate has four associated images. The images along the left side show the profile picture on top and the top-down view on the bottom. The left column corresponds to the BD state while the right is BU.

The CS molecule presents a few interesting avenues for interaction with sumanene. First, the presence of the aromatic ring indicates that dispersion bonding with the benzene rings of sumanene may be important. Electrostatics could also be important because of the electronegativity of the Cl atom and nitrile groups. For the BD configuration, CS binds in a horizontal orientation with the nitrile groups and Cl atom located over the H atoms at the edge of sumanene. The bowl up configuration is similar with a slight difference in the angle at which the CS molecule is interacting with the BU sumanene.

Examining the structure the HDI-sumanene system we see that the HDI conforms to the shape of the adsorbent due to its flexible-nature. For the BD case the molecules wraps along the convex edge with the isocyanate functional groups pointed downward towards the H atoms at the edge of sumanene. From the top-down view we see that the molecule's backbone is situated off-center from the sumanene indicating that there is a preferred interaction with the 5-member rings. In the BU configuration HDI conforms slightly to the concave surface with the isocyanate functional groups pointing slightly upward. The top-down view shows that, unlike the BD case, the HDI molecule is centered over sumanene.

Finally, the structures for TDI-sumanene are shown in the bottom frame. TDI is bound to sumanene with the toluene ring off-center positioned over the bond separating a 5-member and 6-member ring for the BD configuration. The isocyanate groups conform to the shape of sumanane and point slightly downward towards the edge H atoms. The methyl group is located off of the side of molecule showing little contribution to the interaction. In the BU configuration TDI is slightly tilted with the methyl group located almost directly over the center of sumanene. The isocyanate functional groups are off towards the edge in contrast to the BD case. Since sumanene possesses a dipole moment, the expectation would be that the isocyanate groups would be attracted to the center of the BU state, but the optimized configuration indicates that the O-H interaction between isocyanate and the edge H atoms on sumanene are more energetically favorable.

While Figure 14 presents the optimized structures for the adsorption process we see

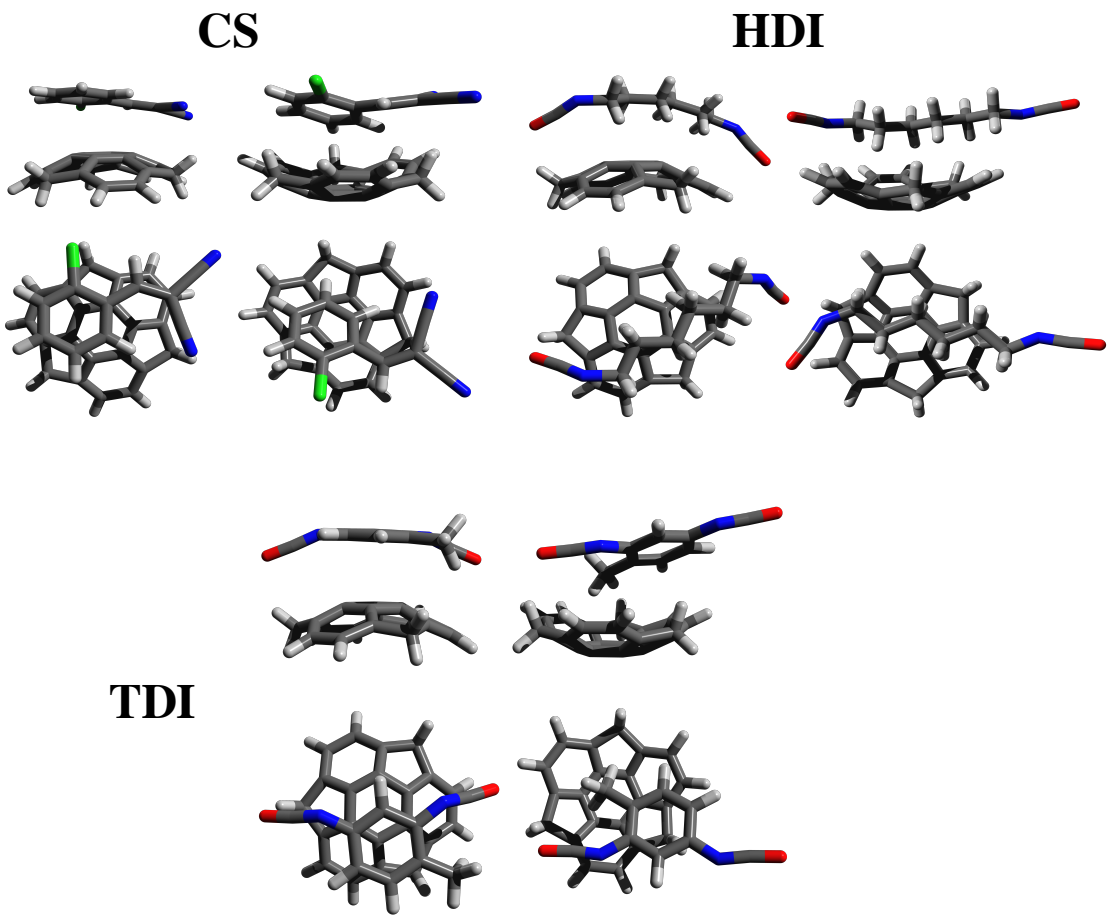


Figure 14: Optimized systems with respiratory irritants on sumanene. Names of the molecules have been abbreviated: 2-Chlorobenzalmalonitrile (CS), 1,6 Hexamethylene Diisocyanate (HDI), and Toluene Diisocyanate (TDI). Profile pictures of the systems are shown along the top rows with top-down views below those. Bowl down (BD) and bowl up (BU) configurations are show. Note that structural distortion occurs due to adsorption for some molecules.

that there are structural changes which occur to the adsorbates in order to reach those configurations. Ideally, adsorption would take place through an adsorbate coming in to contact with the adsorbent through a purely energetically favorable process. However, with the presence of structural changes there is the possibility that an energetic barrier may be present which must be overcome. This barrier would hinder the adsorption interaction and must be investigated to provide the complete picture of the interaction.

Figure 15 shows the energetic profile of each system along the reaction coordinate starting from a system where there is a large distance separating the molecules (right) and finishing with the adsorbed complex (left). The dashed horizontal lines on the plots indicate the combined energy of the fragments when they are infinitely separated. All energies are scaled with respect to this value to indicate the change of energy as the adsorption interaction proceeds.

With the application of the FSM along the reaction coordinate, no significant structural barriers (energies higher than isolated fragments) were found for the adsorbates interacting with the BD and BU states of sumanene. This means that the adsorption interactions are energetically favorable which implies that sumanene would be an adsorbent of interest for these molecules since no extra energy is required to promote adsorption. In general, such barrier may exist if significant conformation changes occur during the adsorption process. Now that the adsorbed structures have been identified and no significant structural barriers were found, the type of interaction can be examined to understand the primary contributors to the interaction energy.

### 4.2.2 Energy Decomposition Analysis

Energy decomposition analysis seeks to decompose an interaction energy in terms of intuitive, easy-to-interpret components. In this case, we employ the EDA method developed by Horn *et al.* which separates the energy into the frozen, polarization, and charge transfer interactions. The frozen component is further broken down into the Pauli, electrostatic, and dispersion contributions using the SCFMI method. Figure 16 displays the results of an EDA perfored for both BD and BU sumanene states for all adsorbates. Note that the components

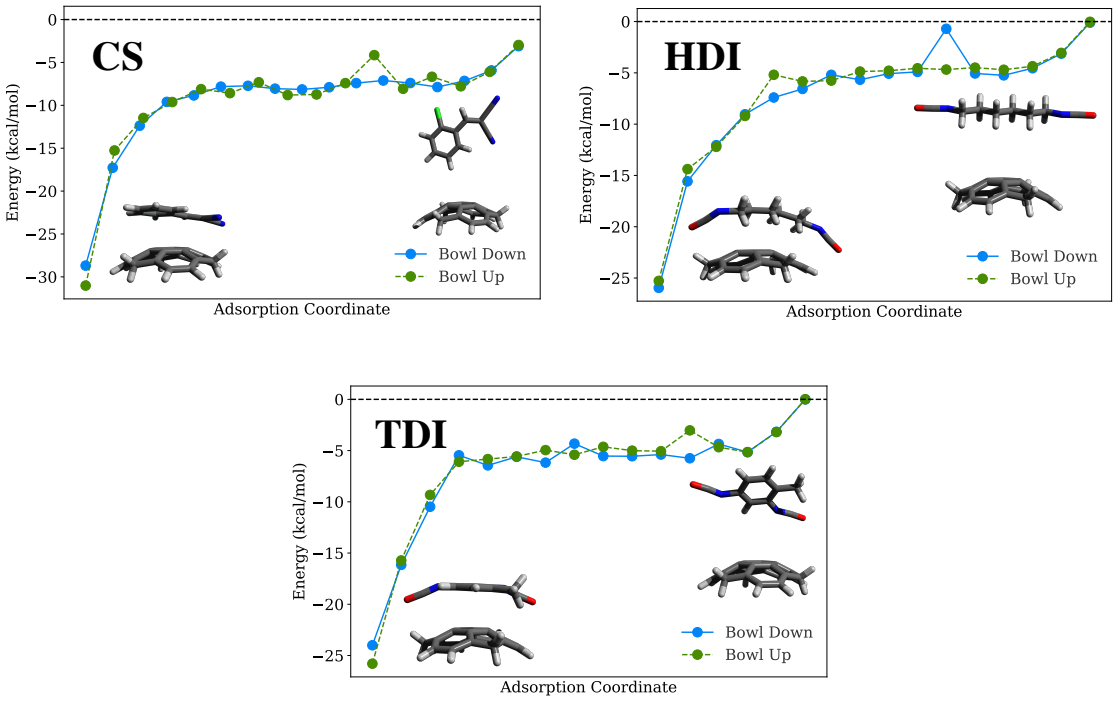


Figure 15: Energies along adsorption coordinate calculated with the freezing string method. Since geometric distortions occur during adsorption, this checks to see if any major energetic barriers need to be overcome. No major structural barriers were found indicating that the molecules can thermally adsorb to the sumanene adsorbent without additional energy.

of the frozen interaction have been separated out and shown next to polarization and charge transfer to give a better understanding of the interplay between Pauli repulsion, attractive dispersion, and electrostatics.

The CS molecule on the left shows a total interaction energy of -13.28 kcal/mol for the BD configuration and -14.3 kcal/mol for BU. The stronger binding in the BU case is due to all of the attractive components being slightly stronger than in the BD case with none in particular distinguishing themselves. Note, that the gains in the attractive components have to overcome the repulsion due to the Pauli component which is larger in the BU state. The interaction energy for both states is largely derived from the electrostatic and dispersion components which balance the Pauli repulsion. Charge transfer and polarization play a very small role.

HDI shows an opposite trend: the BD configuration has a total interaction energy of -14.14 kcal/mol while the BU structure has an energy of -12.86. The driving component of this trend is the Pauli repulsion which is smaller for the BD system. Electrostatics are slightly stronger in the BD state, but this is offset by a larger dispersion component for the BU system. As with the CS-sumanene systems, polarization and charge transfer play only a minor role.

Finally, the EDA of TDI-sumanene is shown on the right. The interaction energy for the BD state is -12.53 kcal/mol while the BU configuration has a total interaction energy of -12.93 giving the BU state a slightly stronger interaction. As with the other molecules, the electrostatic and dispersion components account for most of the binding with Pauli repulsion counterbalancing this interaction. Interestingly, differences between the Pauli repulsion, electrostatics, and dispersion cancel between the BD and BU systems. The difference of the interaction energy is actually a slightly stronger polarization component in the BU configuration. This difference is about 0.48 kcal/mol indicating that a slight polarization of the orbitals drives the change. Charge transfer does not change significantly between systems and contributes little to the interaction.

Among all of the systems we see that the electrostatics and dispersion play the major role of contributing to the attractive component of the interaction energy balancing the Pauli repulsion in the process. While the interaction energies between the BD and BU

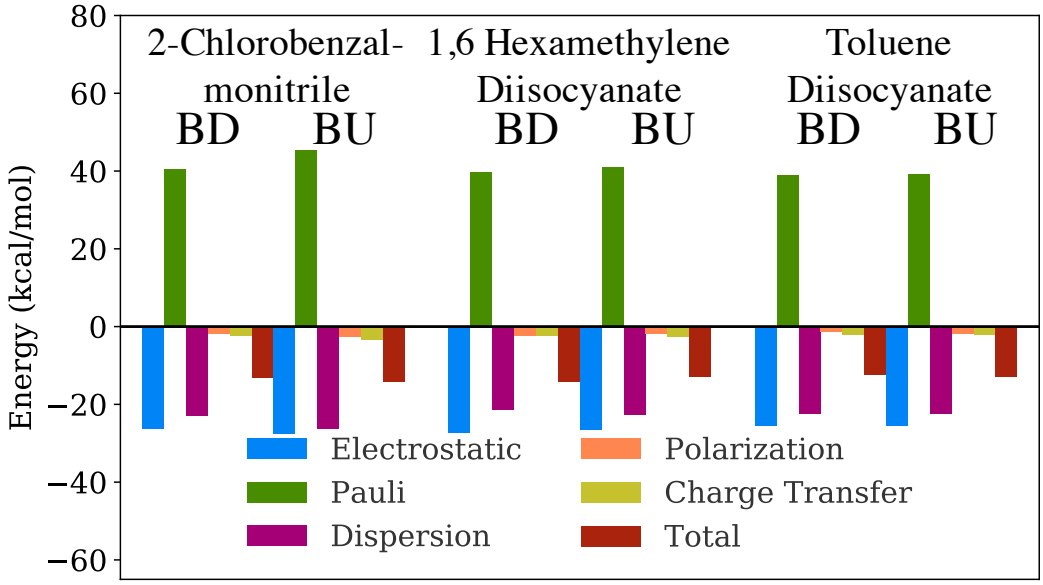


Figure 16: Energy decomposition analysis of respiratory irritants on the bowl down (BD) and bowl up (BU) orientations of sumanene. All molecules were found to be bound largely by electrostatic and dispersion in both the BD and BU states. Charge transfer and polarization played minor roles in the adsorption process. Interestingly, interaction energies between the BD and BU orientation are very similar indicating that the state does not really play a significant role.

configurations is quite similar, small changes occur due to a trade-off of the dispersion and Pauli repulsion, reduction of the Pauli repulsion, and slight changes to the polarization energy. These interactions are explained due to the fact that sumanene possess a dipole moment for electrostatics, and carbon rings to promote dispersion interactions with carbon rings or chains in the adsorbate. These types of interactions are not unique to the molecules chosen, but sumanene appears to act as a good adsorbate based primarily on non-covalent interactions of these respiratory irritants.

## 4.3 Conclusion

This chapter examined the ability of sumanene to act as an adsorbant for three highly potent respiratory irritants. Identifying molecules which act as effective adsorbents for these compounds provides a key insight into developing devices which would help to remove these chemicals from the air to reduce irritation effects and promote a safer work environment. It was found that all three molecules bind to sumanene with an interaction energy between -12.53 kcal/mol and -14.3 kcal/mol which is sufficient to remain adsorbed with low enough thermal energy. The main modes of attraction were found to be electrostatics and dispersion while Pauli repulsion was found to be the largest contributor towards weaker interactions. Through an FSM anaylsis, no significant energetic barriers due to structural rearrangement were found indicating that no extra energy needs to be supplied to the molecules to promote adsorption.

As industries become more complex and new chemicals are discovered, the health hazards which result are largely unknown until a major incident occurs. In particular, respiratory irritants inhibit breathing which can reduce worker effectiveness and lead to long-term health problems if not properly protected. Gas capture/release systems provide a means of reducing the exposure to such gases by removing them from the environment for safe disposal elsewhere. Numerous methods for gas separation exist, but environmental criteria such as operating at room temperature with high selectivity and sensitivity are crucial to operating effectively. With further experimental and device development, surface adsorption systems

such as Buckybowls could offer an energy efficient and chemically tailored means of solving this problem.

# 5.0 Conclusion

> **But when you come right down to it the reason that we did this job is because it was an organic necessity. If you are a scientist you cannot stop such a thing. If you are a scientist you believe that it is good to find out how the world works; that it is good to find out what the realities are; that it is good to turn over to mankind at large the greatest possible power to control the world and to deal with it according to its lights and its values.**
>
> ***J. Robert Oppenheimer***
> *Los Alamos, 1945*

The field of surface adsorption offers promising avenues of research for gas regulation systems through engineering metal organic frameworks, zeolites, and carbon-based capture systems to name a few. This thesis provides a deeper chemical understanding into how Buckybowls can be used for such applications through the use of external electric fields to tune sensitivity and selectivity. Density functional theory and energy decomposition analysis were employed to identify the components of the interaction between small gas molecules and the Buckybowls sumanene and corannulene. Additionally, the components of interaction with three potent sensory irritants were examined in a similar fashion with no external electric field to show that Buckybowls can act as adsorbents to a wide range of molecules.

Interaction energies were presented with the associated energy decomposition analysis for gaseous pollutants $CH_4$, $CO_2$, NO, $NO_2$ and respiratory irritants 2-chlorobenzalmonitrile, 1,6 hexamethylene, and toluene diisocyanate to aid in identifying novel systems for capturing greenhouse gases, atmospheric pollutants, and respiratory irritants. In particular, NO, $NO_2$, and the irritant adsorption on Buckybowls has not been previously reported in the literature as far as the author is aware.

For the small gas molecules, each system was relaxed in the electric field resulting in altered bowl depth. The adjustment in structure and electronic polarization changed interaction energies with respect to the zero-field values. Interestingly, the applied fields affected interaction energies differently across various adsorbates. Several instances were identified where the binding preference for adsorbates was altered by applied fields on specific strengths and directions indicating that the selectivity can be tuned. This phenomenon opens the pos-

sibility of devices composed of Buckybowls to be used as sensitive gas capture/release devices where the strength of the electric field controls the strength of interaction. This work also shed light on the driving forces of adsorbates binding to Buckybowls through EDA. The frozen energy components were identified to be the most largest contributor to the interaction energy for $CH_4$ and $CO_2$ systems, charge transfer was found to play a significant role for NO and $NO_2$.

The frozen fragment energy component was also found to be the dominating factor among interaction energies between sumanene and the respiratory irritants. When decomposed further, dispersion and electrostatics were found to have a similar binding contribution which balanced the Pauli repulsion component. In general, the interaction energies of the irritants were found to be stronger than the small gas molecule systems as expected for adsorbing a larger molecule. Structural changes from the isolated fragment geometries are predicted in the adsorbed configuration among all systems. However, no significant energetic barrier was found indicating that the conformation change would not dramatically affect the adsorption process.

While corannulene and sumanene are the simplest Buckybowls that can be constructed from Buckyballs, there exist many other options in terms of size, structure, and chemical functionality. The Buckybowls studied here represent small, high symmetry Buckbowls, but there are an infinite number of bowl-like molecules that can be synthesized with different shapes and sizes such as semibuckminsterfullerenes [88] to fit a particular adsorbate. The structure of the buckybowl can also be utilized to provide interesting adsorption properties such as harnessing chirality [89, 90] or cavities in templated carbon structures [91, 92]. Another interesting avenue of future research lies in embedding [93] and functionalization of Buckybowls to create specific chemical environments targeting particular adsorbates [94, 26, 95, 96, 97, 98]. Each of these systems offers interesting opportunities for computational research into the adsorption properties for gas molecules due to their unique characteristics and unknown interactions with the wide range of scientifically relevant adsorbates.

Buckybowls represent a class of molecules that show promise for gas adsorption and have the unique characteristic of possessing two states which can be connected via external stimuli. While the present studies are more academic, the results shown here establish the

proof of principle for Buckybowls as stimuli-responsive gas adsorbers and more work will be needed to explore the practical applications of these molecules. The adoption of Buckybowl-based devices requires a significant amount of research such as determining thermal stability of surfaces as well as fabrication of useful devices before it can be used for large scale purposes. With this additional development, Buckybowls offer a fascinating avenue for stimulus-induced gas adsorption and release.

## Appendix: Frozen Components of EDA for Small Gas Molecules

The following figures show the frozen components of the EDA presented in Chapter 3. Throughout all systems it is important to note two points: While the electrostatic contribution is significant with zero applied field, the component becomes energetically unimportant compared to the dispersion and Pauli repulsion. And secondly, the attractive dispersion and Pauli repulsion counter each other as the field is applied. This last result is due to the polarization effect of the electronic wave functions under an applied external field. As the wave functions are driven from the adsorbate to the adsorbent (or *vice versa*) the interaction ranges between the distributions begin to shorten causing a significant increase in strength of these two components.

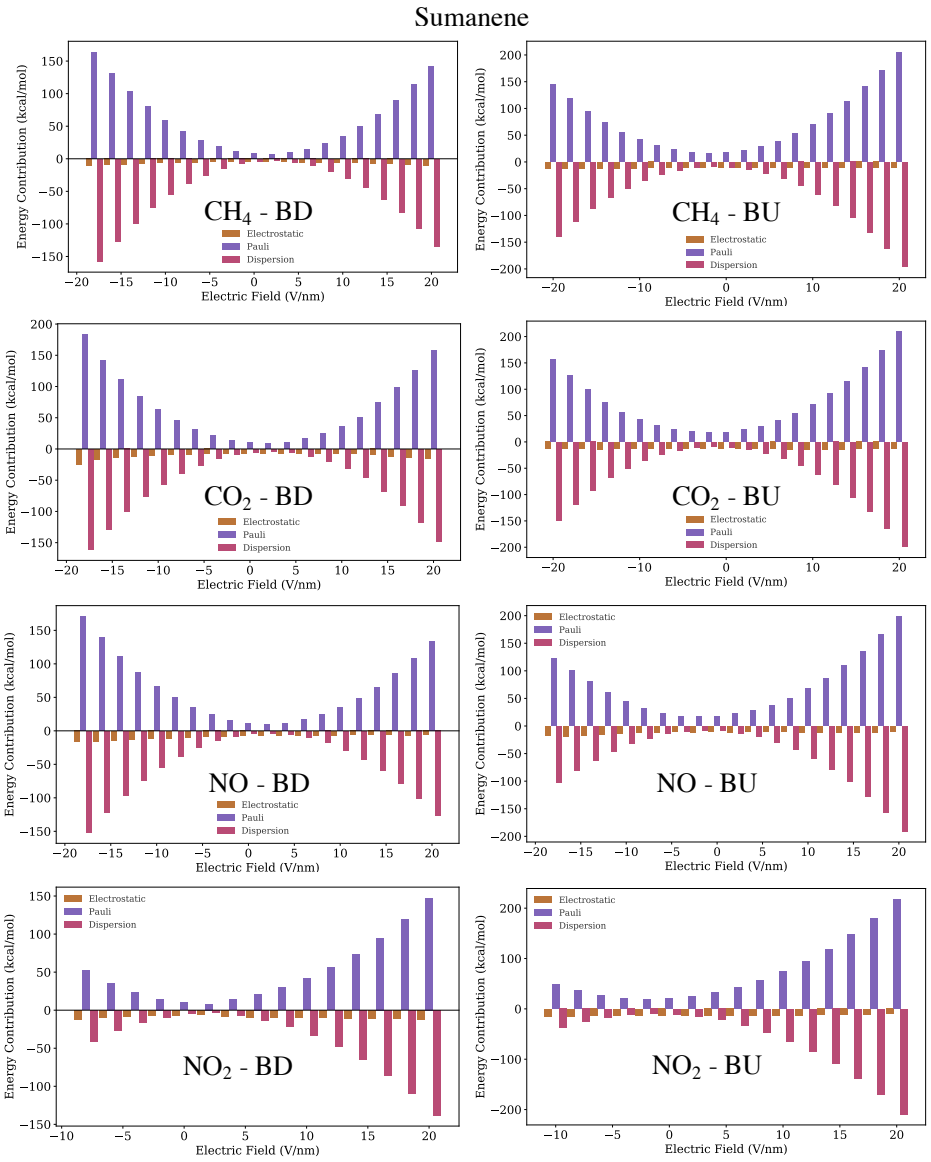


Figure 17: Frozen contribution components of EDA for sumanene. At zero applied electric field, the electrostatic and dispersion components have similar contributions towards attractive interactions. As the magnitude of the field increases, the electrostatic contribution remains nearly constant while the strength of dispersion interactions increase along with the Pauli repulsion component.

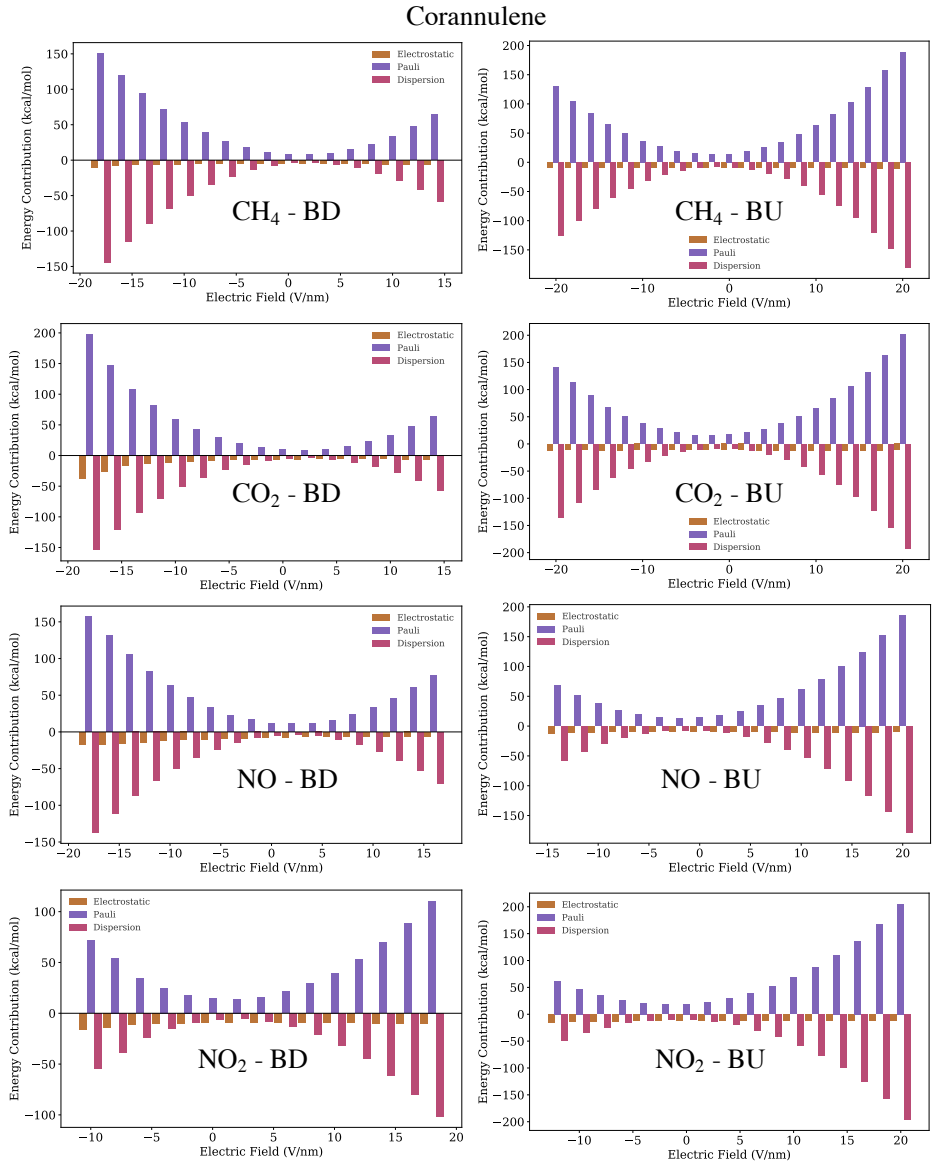


Figure 18: Frozen contribution components of EDA for corannulene. Similarly to sumanene, at zero applied electric field, the electrostatic and dispersion components have similar contributions towards attractive interactions. As the magnitude of the field increases, the electrostatic contribution remains nearly constant while the strength of dispersion interactions increase along with the Pauli repulsion component.

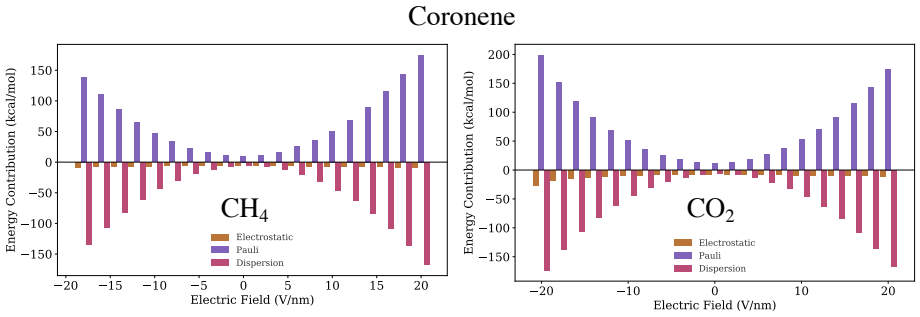


Figure 19: Frozen contribution components of EDA for coronene. Similarly to sumanene, at zero applied electric field, the electrostatic and dispersion components have similar contributions towards attractive interactions. As the magnitude of the field increases, the electrostatic contribution remains nearly constant while the strength of dispersion interactions increase along with the Pauli repulsion component. Note that results for NO and $NO_2$ are not provided due to numerical difficulties with the EDA implementation.

## Bibliography


[1] Harold W Kroto, James R Heath, Sean C O'Brien, Robert F Curl, and Richard E Smalley. C60: Buckminsterfullerene. *nature*, 318(6042):162–163, 1985.

[2] Jan Cami, Jeronimo Bernard-Salas, Els Peeters, and Sarah Elizabeth Malek. Detection of $C_{60}$ and $C_{70}$ in a young planetary nebula. *Science*, 329(5996):1180–1182, 2010.

[3] U.S. Energy Information Administration - EIA - Independent Statistics and Analysis. `https://www.eia.gov/tools/faqs/faq.php?id=77&t=11`.

[4] Carbon Capture and the Future of Coal Power. `https://www.nrg.com/case-studies/petra-nova.html`.

[5] $CO_2$ Recovery Plants: Commercial Experiences. `https://www.mhi.com/products/environment/carbon_dioxide_recovery_process_commercial.html`.

[6] Michele Galizia, Won Seok Chi, Zachary P Smith, Timothy C Merkel, Richard W Baker, and Benny D Freeman. 50th anniversary perspective: polymers and mixed matrix membranes for gas and vapor separation: a review and prospective opportunities. *Macromolecules*, 50(20):7809–7843, 2017.

[7] Lloyd M Robeson. The upper bound revisited. *Journal of membrane science*, 320(1-2):390–400, 2008.

[8] Jian Li, Xiang Zhou, Jing Wang, and Xiufen Li. Two-dimensional covalent organic frameworks (cofs) for membrane separation: a mini review. *Industrial & Engineering Chemistry Research*, 58(34):15394–15406, 2019.

[9] Deanna M D'Alessandro, Berend Smit, and Jeffrey R Long. Carbon dioxide capture: prospects for new materials. *Angewandte Chemie International Edition*, 49(35):6058–6082, 2010.

[10] M Calatayud, A Markovits, M Menetrey, B Mguig, and C Minot. Adsorption on perfect and reduced surfaces of metal oxides. *Catalysis Today*, 85(2-4):125–143, 2003.

[11] Ranjani V Siriwardane, Ming-Shing Shen, Edward P Fisher, and James A Poston. Adsorption of co2 on molecular sieves and activated carbon. *Energy & Fuels*, 15(2):279–284, 2001.

[12] Yalou Guo, Hui Zhang, and Yingshu Liu. Desorption characteristics and kinetic parameters determination of molecular sieve by thermogravimetric analysis/differential thermogravimetric analysis technique. *Adsorption Science & Technology*, 36(7-8):1389–1404, 2018.

[13] Molecular Sieve Z10-02 For Air Purification. `http://www.zettachem.com/pdf/Air_pre%20purification_with_Z10-02.pdf`.

[14] CP Chen, S Mehta, LP Fu, A Petrou, FM Gasparini, and A Hebard. Sorption of helium by Fullerite Crystals and Films. *Physical review letters*, 71(5):739, 1993.

[15] CP Chen, S Mehta, EA Hoefling, S Zelakiewicz, and FM Gasparini. Sorption Studies of Helium and Neon by Crystals of $C_{60}$ and $C_{70}$. *Journal of low temperature physics*, 102(1-2):31–59, 1996.

[16] W Teizer, RB Hallock, and AF Hebard. $^4$He adsorption and Superfluid Transition on $C_{60}$. *Journal of low temperature physics*, 109(1-2):243–265, 1997.

[17] W Teizer, RB Hallock, QM Hudspeth, and AF Hebard. Anomalous $^4$He Adsorption to in situ Baked $C_{60}$. *Journal of low temperature physics*, 113(3-4):453–458, 1998.

[18] W Teizer, RB Hallock, and AF Hebard. Thin Film Adsorption of $^4$He to $C_{60}$. *Journal of Low Temperature Physics*, 110(1-2):647–652, 1998.

[19] Joseph D Turnbull and Massimo Boninsegni. Adsorption of para-hydrogen on fullerenes. *Physical Review B*, 71(20):205421, 2005.

[20] T Coffey and J Krim. Quartz-crystal microbalance studies of the slippage of solid and liquid krypton monolayers on metal (111) and $C_{60}$ surfaces. *Physical Review B*, 72(23):235414, 2005.

[21] RA Trasca, Milton Walter Cole, T Coffey, and J Krim. Gas adsorption on a $C_{60}$ monolayer. *Physical Review E*, 77(4):041603, 2008.

[22] Wayne E Barth and Richard G Lawton. Dibenzo [ghi, mno] fluoranthene. *Journal of the American Chemical Society*, 88(2):380–381, 1966.

[23] Anna M Butterfield, Bruno Gilomen, and Jay S Siegel. Kilogram-scale production of corannulene. *Organic Process Research & Development*, 16(4):664–676, 2012.

[24] Hidehiro Sakurai, Taro Daiko, and Toshikazu Hirao. A synthesis of sumanene, a fullerene fragment. *Science*, 301(5641):1878–1878, 2003.

[25] Toru Amaya, Takanori Ito, Shun Katoh, and Toshikazu Hirao. Regioselective functionalization of sumanene. *Tetrahedron*, 71(35):5906–5909, 2015.

[26] Andrzej Sygula. Chemistry on a half-shell: Synthesis and derivatization of buckybowls. *European Journal of Organic Chemistry*, 2011(9):1611–1625, 2011.

[27] Xu Li, Feiyu Kang, and Michio Inagaki. Buckybowls: Corannulene and its derivatives. *Small*, 12(24):3206–3223, 2016.

[28] Lawrence T Scott, Mohammed M Hashemi, and Matthew S Bratcher. Corannulene bowl-to-bowl inversion is rapid at room temperature. *Journal of the American Chemical Society*, 114(5):1920–1921, 1992.

[29] T Jon Seiders, Kim K Baldridge, Gunther H Grube, and Jay S Siegel. Structure/energy correlation of bowl depth and inversion barrier in corannulene derivatives: combined experimental and quantum mechanical analysis. *Journal of the American Chemical Society*, 123(4):517–525, 2001.

[30] Toru Amaya, Hiroyuki Sakane, Toshiko Muneishi, and Toshikazu Hirao. Bowl-to-bowl inversion of sumanene derivatives. *Chemical communications*, (6):765–767, 2008.

[31] Rached Jaafar, Carlo A Pignedoli, Giovanni Bussi, Kamel Ait-Mansour, Oliver Groening, Toru Amaya, Toshikazu Hirao, Roman Fasel, and Pascal Ruffieux. Bowl inversion of surface-adsorbed sumanene. *Journal of the American Chemical Society*, 136(39):13666–13671, 2014.

[32] Shintaro Fujii, Maxim Ziatdinov, Shuhei Higashibayashi, Hidehiro Sakurai, and Manabu Kiguchi. Bowl inversion and electronic switching of buckybowls on gold. *Journal of the American Chemical Society*, 138(37):12142–12149, 2016.

[33] M Althaf Hussain, Dolly Vijay, and G Narahari Sastry. Buckybowls as adsorbents for co2, ch4, and c2h2: Binding and structural insights from computational study. *Journal of computational chemistry*, 37(3):366–377, 2016.

[34] Stevan Armaković, Sanja J Armaković, Jovan P Šetrajčić, Stevo K Jaćimovski, and Vladimir Holodkov. Sumanene and its adsorption properties towards co, co 2 and nh 3 molecules. *Journal of molecular modeling*, 20(4):2170, 2014.

[35] Niels Bohr. On the constitution of atoms and molecules. *The London, Edinburgh, and Dublin Philosophical Magazine and Journal of Science*, 26(153):476–502, 1913.

[36] Douglas Rayner Hartree and W Hartree. Self-consistent field, with exchange, for beryllium. *Proceedings of the Royal Society of London. Series A-Mathematical and Physical Sciences*, 150(869):9–33, 1935.

[37] John A Pople, D Po Santry, and Gerald A Segal. Approximate self-consistent molecular orbital theory. i. invariant procedures. *The Journal of Chemical Physics*, 43(10):S129–S135, 1965.

[38] JA Pople, DL Beveridge, and PA Dobosh. Approximate self-consistent molecular-orbital theory. v. intermediate neglect of differential overlap. *The Journal of Chemical Physics*, 47(6):2026–2033, 1967.

[39] John A Pople and Warren J Hehre. Computation of electron repulsion integrals involving contracted gaussian basis functions. *Journal of Computational Physics*, 27(2):161–168, 1978.

[40] Martin Head-Gordon and John A Pople. A method for two-electron gaussian integral and integral derivative evaluation using recurrence relations. *The Journal of chemical physics*, 89(9):5777–5786, 1988.

[41] Peter MW Gill, Benny G Johnson, and John A Pople. Two-electron repulsion integrals over gaussian s functions. *International journal of quantum chemistry*, 40(6):745–752, 1991.

[42] WJ Hehre, WA Lathan, R Ditchfield, M_ D Newton, and JA Pople. Gaussian 70: Ab initio scf-mo calculations on organic molecules. *Quantum Chem. Program Exch*, 11:236, 1973.

[43] Daniel Burrill. Density functional theory study of dilute transition metal phthalocyanines. 2015.

[44] John C Slater. A simplification of the hartree-fock method. *Physical review*, 81(3):385, 1951.

[45] Pierre Hohenberg and Walter Kohn. Inhomogeneous electron gas. *Physical review*, 136(3B):B864, 1964.

[46] Walter Kohn and Lu Jeu Sham. Self-consistent equations including exchange and correlation effects. *Physical review*, 140(4A):A1133, 1965.

[47] Jos Thijssen. *Computational physics*. Cambridge university press, 2007.

[48] S F_ Boys and FJMP Bernardi. The calculation of small molecular interactions by the differences of separate total energies. some procedures with reduced errors. *Molecular Physics*, 19(4):553–566, 1970.

[49] Kazuo Kitaura and Keiji Morokuma. A new energy decomposition scheme for molecular interactions within the hartree-fock approximation. *International Journal of Quantum Chemistry*, 10(2):325–340, 1976.

[50] Bogumil Jeziorski, Robert Moszynski, and Krzysztof Szalewicz. Perturbation theory approach to intermolecular potential energy surfaces of van der waals complexes. *Chemical Reviews*, 94(7):1887–1930, 1994.

[51] Joseph O Hirschfelder and W Byers Brown. Perturbation theory. *Advances in quantum chemistry*, page 255, 1964.

[52] Rustam Z Khaliullin, Erika A Cobar, Rohini C Lochan, Alexis T Bell, and Martin Head-Gordon. Unravelling the origin of intermolecular interactions using absolutely localized molecular orbitals. *The Journal of Physical Chemistry A*, 111(36):8753–8765, 2007.

[53] E Gianinetti, M Raimondi, and E Tornaghi. Modification of the roothaan equations to exclude bsse from molecular interaction calculations. *International journal of quantum chemistry*, 60(1):157–166, 1996.

[54] Takeshi Nagata, Osamu Takahashi, Ko Saito, and Suehiro Iwata. Basis set superposition error free self-consistent field method for molecular interaction in multicomponent systems: Projection operator formalism. *The Journal of Chemical Physics*, 115(8):3553–3560, 2001.

[55] Paul R Horn, Yuezhi Mao, and Martin Head-Gordon. Probing non-covalent interactions with a second generation energy decomposition analysis using absolutely localized molecular orbitals. *Physical Chemistry Chemical Physics*, 18(33):23067–23079, 2016.

[56] Ed Dlugokencky. Global $co_2$ monthly means. `https://www.esrl.noaa.gov/gmd/ccgg/trends/gl_data.html`. NOAA/ESRL.

[57] Ed Dlugokencky. Global $ch_4$ monthly means. `https://www.esrl.noaa.gov/gmd/ccgg/trends_ch4/`. NOAA/ESRL.

[58] Leif Hockstad and L Hanel. Inventory of us greenhouse gas emissions and sinks. Technical report, Environmental System Science Data Infrastructure for a Virtual Ecosystem, 2018.

[59] John H Seinfeld and Spyros N Pandis. *Atmospheric chemistry and physics: from air pollution to climate change*. John Wiley & Sons, 2016.

[60] Di Price, Rona Birnbaum, Richard Batiuk, Melissa McCullough, and Roy Smith. Nitrogen oxides: Impacts on public health and the environment. Technical report, Environmental Protection Agency, Washington, DC (United States)., 1997.

[61] Richard W Baker. Future directions of membrane gas separation technology. *Industrial & engineering chemistry research*, 41(6):1393–1411, 2002.

[62] Richard W Baker. *Membrane technology and applications*. John Wiley & Sons, 2012.

[63] Jennifer Wilcox. *Carbon capture*. Springer Science & Business Media, 2012.

[64] Wojciech M Budzianowski. *Energy Efficient Solvents for CO2 Capture by Gas-Liquid Absorption: Compounds, Blends and Advanced Solvent Systems*. Springer, 2016.

[65] Pluton Pullumbi, Federico Brandani, and Stefano Brandani. Gas separation by adsorption: technological drivers and opportunities for improvement. *Current Opinion in Chemical Engineering*, 24:131–142, 2019.

[66] Hongyan Guo, Wenhua Zhang, Ning Lu, Zhiwen Zhuo, Xiao Cheng Zeng, Xiaojun Wu, and Jinlong Yang. Co2 capture on h-bn sheet with high selectivity controlled by external electric field. *The Journal of Physical Chemistry C*, 119(12):6912–6917, 2015.

[67] L Valentini, I Armentano, JM Kenny, Carlo Cantalini, Luca Lozzi, and Sandro Santucci. Sensors for sub-ppm no 2 gas detection based on carbon nanotube thin films. *Applied Physics Letters*, 82(6):961–963, 2003.

[68] Sandro Santucci, S Picozzi, F Di Gregorio, Luca Lozzi, Carlo Cantalini, L Valentini, JM Kenny, and B Delley. No 2 and co gas adsorption on carbon nanotubes: experiment and theory. *The Journal of chemical physics*, 119(20):10904–10910, 2003.

[69] Shu Peng, Kyeongjae Cho, Pengfei Qi, and Hongjie Dai. Ab initio study of cnt no2 gas sensor. *Chemical Physics Letters*, 387(4-6):271–276, 2004.

[70] Hamid Ghorbani Shiraz, Fatemeh Razi Astaraei, Somayeh Fardindoost, and Zahra Sadat Hosseini. Decorated cnt based on porous silicon for hydrogen gas sensing at room temperature. *RSC Advances*, 6(50):44410–44414, 2016.

[71] ZM Ao, J Yang, S Li, and Q Jiang. Enhancement of co detection in al doped graphene. *Chemical Physics Letters*, 461(4-6):276–279, 2008.

[72] Jiayu Dai, Jianmin Yuan, and Paolo Giannozzi. Gas adsorption on graphene doped with b, n, al, and s: a theoretical study. *Applied Physics Letters*, 95(23):232105, 2009.

[73] K Christian Kemp, Humaira Seema, Muhammad Saleh, Nhien H Le, Kandula Mahesh, Vimlesh Chandra, and Kwang S Kim. Environmental applications using graphene composites: water remediation and gas adsorption. *Nanoscale*, 5(8):3149–3171, 2013.

[74] Zhu-Yin Sui, Yue-Na Meng, Pei-Wen Xiao, Zhi-Qiang Zhao, Zhi-Xiang Wei, and Bao-Hang Han. Nitrogen-doped graphene aerogels as efficient supercapacitor electrodes and gas adsorbents. *ACS applied materials & interfaces*, 7(3):1431–1438, 2015.

[75] Stevan Armaković, Sanja J Armaković, and Jovan P Šetrajčić. Hydrogen storage properties of sumanene. *international journal of hydrogen energy*, 38(27):12190–12198, 2013.

[76] Stevan Armaković, Sanja J Armaković, Svetlana Pelemiš, and Dragoljub Mirjanić. Influence of sumanene modifications with boron and nitrogen atoms to its hydrogen adsorption properties. *Physical Chemistry Chemical Physics*, 18(4):2859–2870, 2016.

[77] Adel Reisi-Vanani and Somayeh Mehrdoust. Effect of boron doping in sumanene frame toward hydrogen physisorption: A theoretical study. *International Journal of Hydrogen Energy*, 41(34):15254–15265, 2016.

[78] Yihan Shao, Zhengting Gan, Evgeny Epifanovsky, Andrew TB Gilbert, Michael Wormit, Joerg Kussmann, Adrian W Lange, Andrew Behn, Jia Deng, Xintian Feng, et al. Advances in molecular quantum chemistry contained in the q-chem 4 program package. *Molecular Physics*, 113(2):184–215, 2015.

[79] Piotr De Silva and Clemence Corminboeuf. Simultaneous visualization of covalent and noncovalent interactions using regions of density overlap. *Journal of chemical theory and computation*, 10(9):3745–3756, 2014.

[80] CC Lushbaugh, JW Green Jr, and C Redemann. Effects of prolonged inhalation of oil fogs on experimental animals. *Arch. Indust. Hyg. & Occupational Med.*, 1(2):237–47, 1950.

[81] Yves Alarie. Sensory irritation by airborne chemicals. *CRC critical reviews in toxicology*, 2(3):299–363, 1973.

[82] Michelle Schaper. Development of a database for sensory irritants and its use in establishing occupational exposure limits. *American Industrial Hygiene Association Journal*, 54(9):488–544, 1993.

[83] Ben B Corson and Roger W Stoughton. Reactions of alpha, beta-unsaturated dinitriles. *Journal of the American Chemical Society*, 50(10):2825–2837, 1928.

[84] Rafał Borusiewicz. Detection and identification of traces of lachrymatory incapacitating agents-case studies. *Problems of forensic sciences*, 114:119–135, 2018.

[85] Xiao Lian and Bing Yan. A dual-functional bimetallic-organic framework nanosensor for detection and decontamination of lachrymator in drinking water. *Sensors and Actuators B: Chemical*, 281:168–174, 2019.

[86] Narbe Mardirossian and Martin Head-Gordon. $\omega$ b97m-v: A combinatorially optimized, range-separated hybrid, meta-gga density functional with vv10 nonlocal correlation. *The Journal of chemical physics*, 144(21):214110, 2016.

[87] Andrew Behn, Paul M Zimmerman, Alexis T Bell, and Martin Head-Gordon. Efficient exploration of reaction paths via a freezing string method. *The Journal of chemical physics*, 135(22):224108, 2011.

[88] Peter W Rabideau, Atteye H Abdourazak, Haskell E Folsom, Zbigniew Marcinow, Andrzej Sygula, and Renata Sygula. Buckybowls: Synthesis and ab initio calculated structure of the first semibuckminsterfullerene. *Journal of the American Chemical Society*, 116(17):7891–7892, 1994.

[89] Shuhei Higashibayashi and Hidehiro Sakurai. Asymmetric synthesis of a chiral buckybowl, trimethylsumanene. *Journal of the American Chemical Society*, 130(27):8592–8593, 2008.

[90] Qitao Tan, Shuhei Higashibayashi, Sangita Karanjit, and Hidehiro Sakurai. Enantioselective synthesis of a chiral nitrogen-doped buckybowl. *Nature communications*, 3(1):1–6, 2012.

[91] Hirotomo Nishihara, Quan-Hong Yang, Peng-Xiang Hou, Masashi Unno, Seigo Yamauchi, Riichiro Saito, Juan I Paredes, Amelia Martínez-Alonso, Juan MD Tascón, Yohei Sato, et al. A possible buckybowl-like structure of zeolite templated carbon. *Carbon*, 47(5):1220–1230, 2009.

[92] Hiroyuki Itoi, Hirotomo Nishihara, Takafumi Ishii, Khanin Nueangnoraj, Raul Berenguer-Betrian, and Takashi Kyotani. Large pseudocapacitance in quinone-functionalized zeolite-templated carbon. *Bulletin of the Chemical Society of Japan*, 87(2):250–257, 2014.

[93] Hiroki Yokoi, Yuya Hiraoka, Satoru Hiroto, Daisuke Sakamaki, Shu Seki, and Hiroshi Shinokubo. Nitrogen-embedded buckybowl and its assembly with c 60. *Nature communications*, 6(1):1–9, 2015.

[94] Guopin Xu, Andrzej Sygula, Zbigniew Marcinow, and Peter W Rabideau. Chemistry on the rim of buckybowls: derivatization of 1, 2, 5, 6-tetrabromocorannulene. *Tetrahedron Letters*, 41(51):9931–9934, 2000.

[95] Bernd M Schmidt and Dieter Lentz. Syntheses and properties of buckybowls bearing electron-withdrawing groups. *Chemistry Letters*, 43(2):171–177, 2014.

[96] Yu-Min Liu, Dan Xia, Bo-Wei Li, Qian-Yan Zhang, Tsuneaki Sakurai, Yuan-Zhi Tan, Shu Seki, Su-Yuan Xie, and Lan-Sun Zheng. Functional sulfur-doped buckybowls and their concave–convex supramolecular assembly with fullerenes. *Angewandte Chemie International Edition*, 55(42):13047–13051, 2016.

[97] Niti Ngamsomprasert, Jing-Shuang Dang, Shuhei Higashibayashi, Yumi Yakiyama, and Hidehiro Sakurai. Sumanene derivatives functionalized at the internal carbon. *Chemical Communications*, 53(4):697–700, 2017.

[98] Olena Papaianina, Vladimir A Akhmetov, Alexey A Goryunkov, Frank Hampel, Frank W Heinemann, and Konstantin Y Amsharov. Synthesis of rationally halogenated buckybowls by chemoselective aromatic c- f bond activation. *Angewandte Chemie International Edition*, 56(17):4834–4838, 2017.